Supplementary Information

General methods and instrumentation S2
Computational methods S2
Synthesis and characterization S3
Figures S1-S6. NMR spectra for **2a** S1-S8
Figure S7. HRMS spectrum for **2a** S9
Figures S8-S13. NMR spectra for **2b** S11-S15
Figure S14. HRMS spectrum for **2b** S16
Figures S15-S19. NMR spectra for **3a** S17-S20
Figure S20. HRMS spectrum for **3a** S21
Figures S21-S22. NMR spectra for **3b** S22-S23
Figure S23. HRMS spectrum for **3b** S23
Figures S24-S27. NMR spectra for **3c** S24-S26
Figure S28. HRMS spectrum for **3c** S27
Figure S29. Chiral stationary phase HPLC profiles of **2b** S27
Figure S30. Experimental and TD-DFT simulated CD and UV-vis spectra for **2b**. S28
Figure S31. Experimental and TD-DFT simulated electronic spectra of **2a** and **3a**. S29
Table S1. TD-DFT Calculated Electronic Transitions for **2a** S30
Table S2. TD-DFT Calculated Electronic Transitions for **3a** S32
Table S3. NICS(*z*) for DFT-optimized structures of **2a**, **3a**, **1b**, **1c** S36
Figure S32. NICS values for **2a**, **3a**, **1b**, and **1c** calculated at different distances from the mean planes of the rings. S37
Table S4. Computational details S37
Figure S33. Cyclic and differential pulse voltammograms of **2a** S38
Figure S34. Cyclic and differential pulse voltammograms of **2b** S39
Figure S35. Cyclic and differential pulse voltammograms of **3a** S40
Figure S36. Cyclic and differential pulse voltammograms of **3b** S41
Figure S37. Cyclic and differential pulse voltammograms of **3c** S42
Figure S38. Energies of Kohn-Sham frontier orbitals calculated for **2a**, **3a**, and **1b** S43
Reference List S43

General methods and instrumentation

Commercial reagents were used without further purification. Solvents were freshly distilled from the appropriate drying agents or purified under nitrogen with the mBraun MBSPS-800 before use. The analytical TLCs were performed with silica gel 60 F254 plates. Column chromatography was performed by using silica gel 60 (200-300 mesh ASTM). The NMR spectra were recorded on a Bruker Avance II spectrometer, operating at 500 MHz for ^{1}H and 125 MHz for ^{13}C or a Bruker Avance II spectrometer operating at 600 MHz for ^{1}H and 150 MHz for ^{13}C. TMS was used as an internal reference for ^{1}H and ^{13}C chemical shifts and $CDCl_3$ was used as solvent. Standard pulse programs from the Bruker library were used for homo- and heteronuclear 2D experiments. Mass spectrometry measurements were conducted by using the electrospray ionization technique on a Bruker Daltonics microTOF-Q. Absorption UV/Vis/NIR spectra were recorded by using a Varian Cary 50 Bio and Jasco V-770 spectrophotometers. HPLC separations were carried out by means of Chirex 3010 analytical column (25 cm length, 4.6 mm i.d.) packed with 5 mm silica gel coated with covalently bound (S)-valine and dinitroaniline using Shimadzu chromatographic system or Merck-Hitachi LaChrom series connected to a flow-cell mounted on Jasco J-1500 spectropolarimeter. HPLC-grade hexane was used. The applied dichloromethane was freshly distilled over calcium hydride. Circular dichroism spectra were obtained directly in the flow cell by means of pseudo stopped-flow technique using a Jasco J-1500 spectropolarimeter. Electrochemical measurements were performed by means of Autolab (Metrohm) potentiostat/galvanostat system for dichloromethane solutions with a glassy carbon, a platinum wire, and Ag/AgCl as the working, auxiliary, and reference electrodes, respectively. Tetrabutylammonium hexafluorophosphate was used as a supporting electrolyte. The potentials were referenced with the ferrocene/ferrocenium couple used as an internal standard. X-ray diffraction data of the single crystals were collected at 100 K. The structures were solved by direct methods with SHELXS97[1] and refined by the full-matrix least-squares method on all F^2 data by using the SHELXL-2016/6 incorporated in the shelXle program[1;2]. All hydrogen atoms, including those located in the difference density map, were placed in calculated positions and refined as the riding model.

Computational methods

Density functional theory (DFT) calculations were performed by using the Gaussian 09 program[3]. DFT geometry optimizations were carried out in the unconstrained C_1 symmetry by using the X-ray structure, molecular mechanics, or semiempirical models as starting geometries. DFT geometries were refined to meet standard convergence criteria, and the existence of a local minimum was verified by a normal mode frequency calculation. DFT calculations were performed by using the hybrid B3LYP functional[4-6] functional combined with the 6-31G(d,p) basis set. The electronic spectra were simulated by means of time-dependent density functional theory (TD-DFT) using the Tamm-Dancoff approximation for 50 states. For TD calculations, the polarizable continuum model of solvation was used (PCM, standard dichloromethane parametrization). The electronic transitions and UV/Vis/NIR as well as CD spectra were analyzed by means of the GaussSum program.[9] The transitions were convoluted by Gaussian curves with 2000 cm^{-1} half line width. NICS calculations were performed for gas phase energies and densities obtained at the B3LYP/6-31G(d,p) level of theory.

Synthesis and characterization

Synthesis of the precursor. 5,15-dimesityl-norcorrolatonickel(II) (**1**) was synthesized and purified according to a literature method.[10]

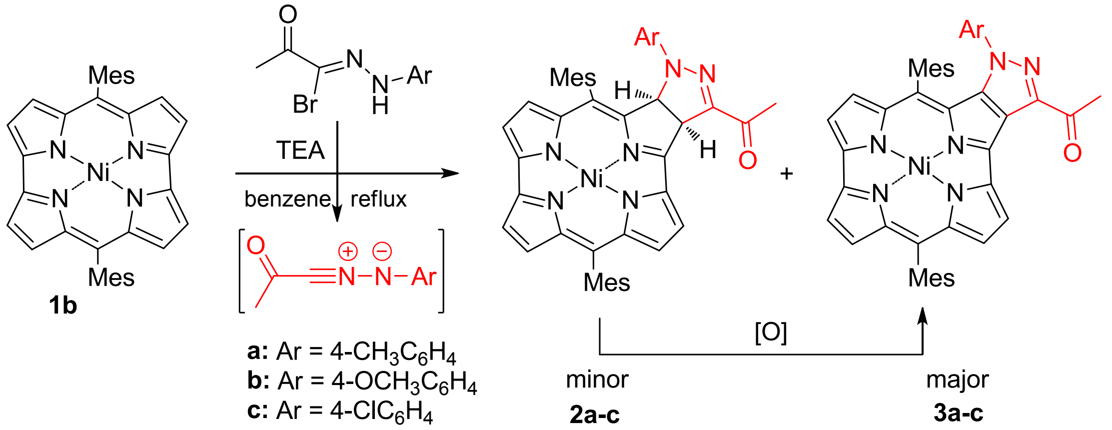

A general synthetic procedure. A solution of Ni-norcorrole **1b** (58 mg, 0.1 mmol), hydrazonoyl bromides (0.15 mmol) and tiethylamine (30 mg, 0.3 mmol) in 10 mL benzene was stirred at 70°C for 2 h under the protection of N_2. The reaction progress was monitored by TLC. The solvent was then evaporated under vacuum. The residue was chromatographed on a silica gel column with dichloromethane as eluent to afford the desired products **2a+3a** in 63% yield, **2b+3b** in 60% yield and **2c+3c** in 65% yield. The products **2** were partially oxidized to **3** in column chromatograph process. The **2+3** mixture was further separated by chiral-phase HPLC (Chirex 3010 analytical column, 25 cm length, 4.6 mm i.d.), injection: 0.5 mg/100 μL, mobile phase: hexane/CH_2Cl_2 (v/v = 15:85), 2 mL/min, detection at λ = 620 nm) to get pure **2** and **3** (yields: 30% for **2a**, 70% for **3a**; 27% for **2b**, 83% for **3b**, estimated on the basis of the HPLC peak integrations)**. 2c** was not obtained due to its oxidation to **3c** in purification process.

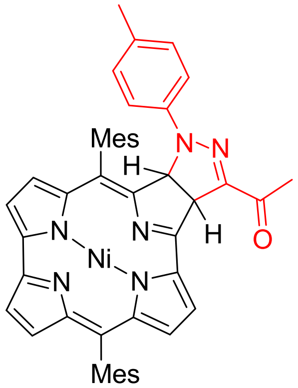

Selected data for **2a**. ^{1}H NMR (500MHz, $CDCl_3$, 298K) δ = 1.41 (s, 3H, $-CH_3$), 2.02 (s, 3H, $-CH_3$), 2.06 (s, 3H, $-CH_3$), 2.09 (s, 3H, $-CH_3$), 2.14 (s, 3H, $-CH_3$), 2.21 (s, 3H, $-CH_3$), 2.75 (d, *J* = 3.5 Hz, 1H, pyrrH), 2.95 (s, 6H, $-CH_3$), 3.12 (d, *J* = 10.0 Hz, 1H, pyrrH), 3.17 (d, *J* = 4.0 Hz, 1H, pyrrH), 3.62 (d, *J* = 5.0 Hz, 1H, pyrrH), 3.65 (d, *J* = 3.5 Hz, 1H, pyrrH), 3.67 (d, *J* = 10.0 Hz, 1H, pyrrH), 3.73 (d, *J* = 5.0 Hz, 1H, pyrrH), 4.31 (d, *J* = 4.0 Hz, 1H, pyrrH), 6.00 (d, *J* = 8.5 Hz, 2H, ArH), 6.03 (s, 1H, ArH), 6.46 (s, 1H, ArH), 6.52 (d, *J* = 8.5 Hz, 2H, ArH), 6.60 (s, 1H, ArH), 6.68 (s, 1H, ArH). ^{13}C NMR (125MHz, $CDCl_3$, 298 K) δ_c = 17.7 ($-CH_3$), 18.2 ($-CH_3$), 19.4 ($-CH_3$), 19.5 ($-CH_3$), 20.7 ($-CH_3$), 20.75 ($-CH_3$), 20.8 ($-CH_3$), 24.9 ($-CH_3$), 53.7 (pyrrC), 66.3 (pyrrC), 115.6, 117.7, 118.3, 118.4, 121.1, 121.4, 127.9, 128.1, 128.7, 129.2, 129.3, 129.6, 133.0, 134.1, 134.7, 135.5, 136.8, 137.1, 137.4, 138.2, 138.4, 138.9, 139.0, 142.6, 142.7, 146.9, 147.2, 147.8, 148.5, 171.3, 174.6, 190.9 (acetyl C=O). UV-vis (CH_2Cl_2) λ_{max}/nm (logε): 337 (4.38), 420 (sh), 471 (sh). ESI-HRMS calc. for $[C_{46}H_{40}N_6NiO]^+$ (M^+): 750.2612, Found: 750.2590.

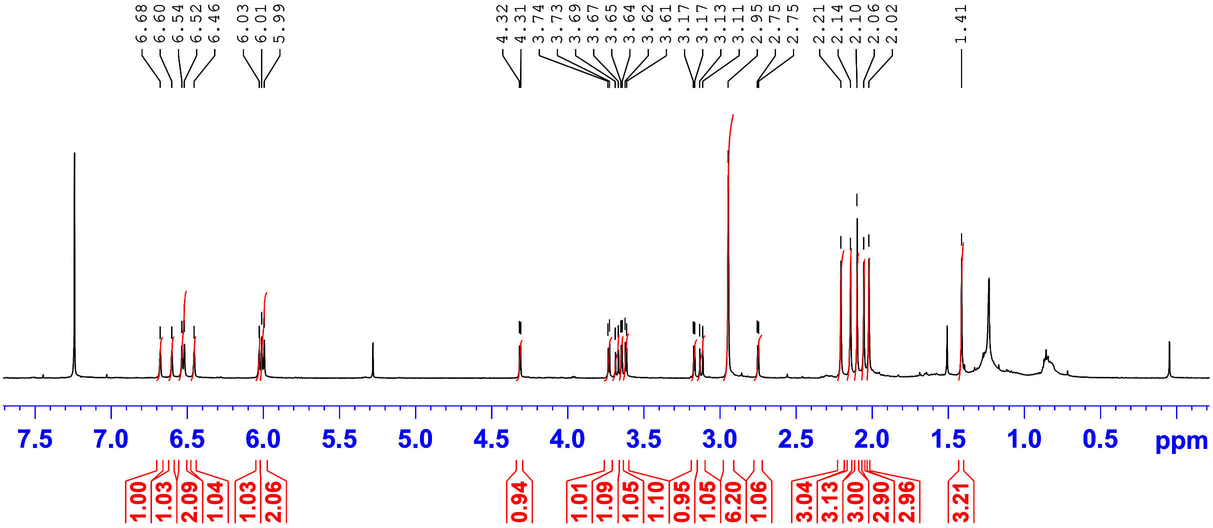

Figure S1. ^{1}H NMR spectrum (500 MHz, $CDCl_3$, 300 K) of **2a**. S – residual $CHCl_3$ signal, * - impurities.

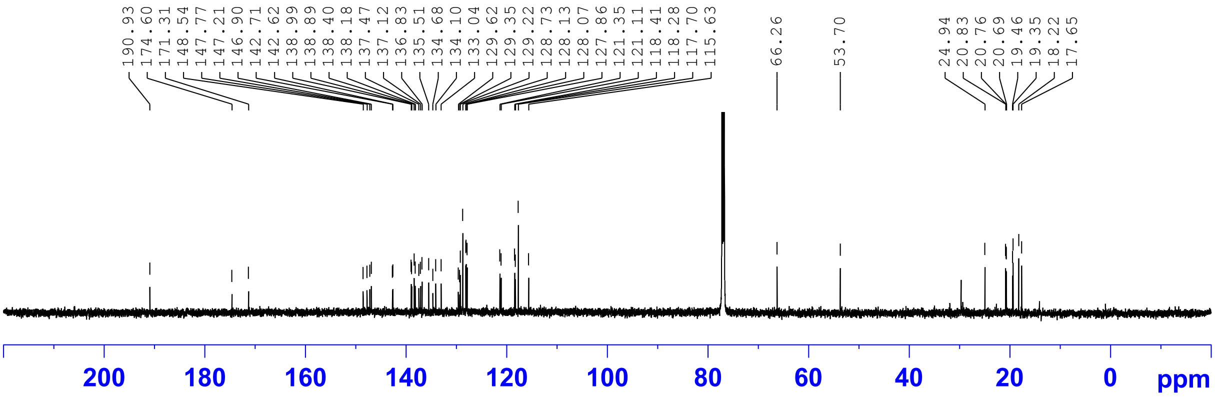

Figure S2. ^{13}C NMR spectrum (126 MHz, CDCl$_3$, 300 K) of **2a**. * - impurities.

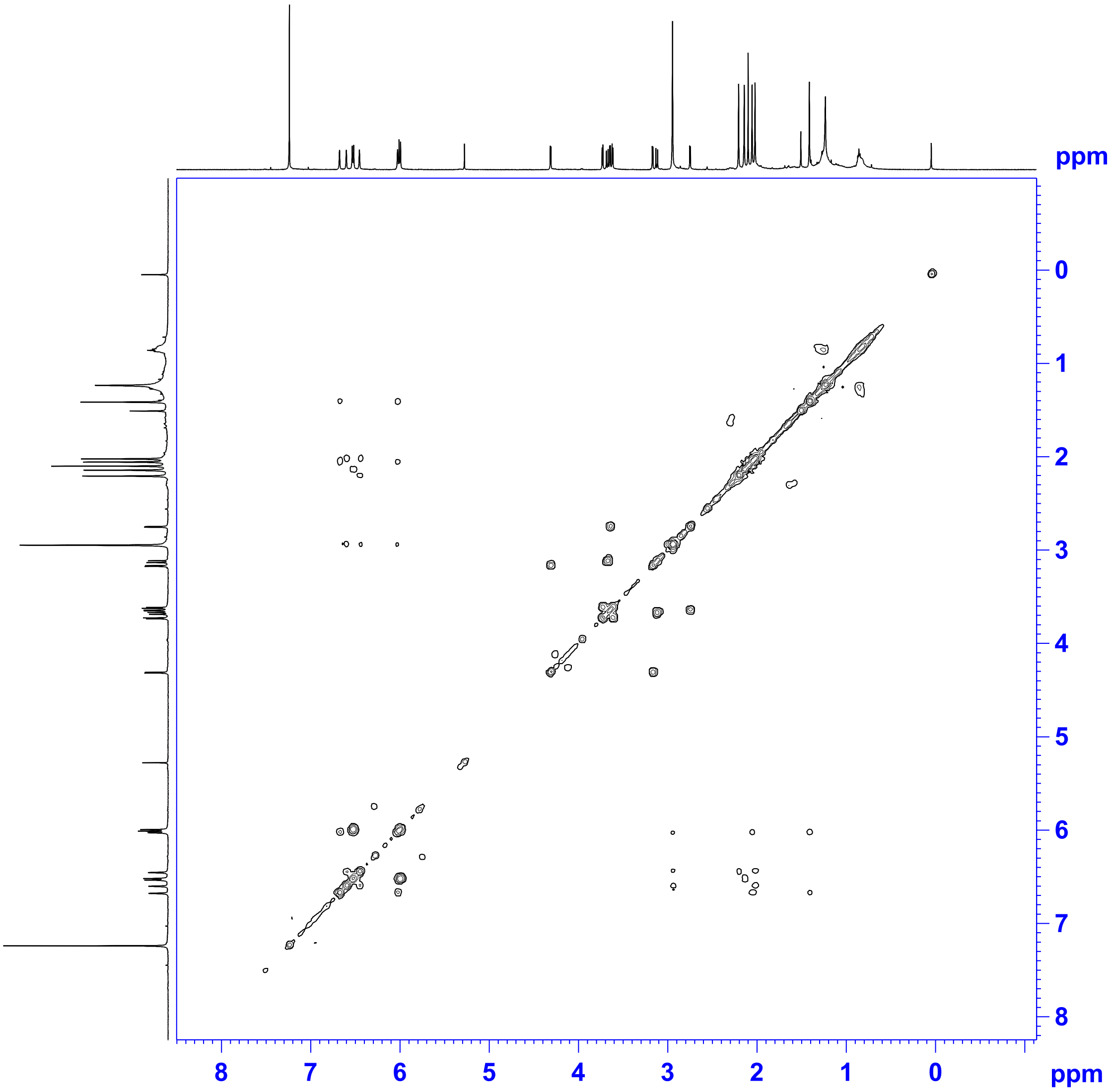

Figure S3. ^{1}H,^{1}H COSY spectrum (500 MHz, CDCl$_3$, 300 K) of **2a**.

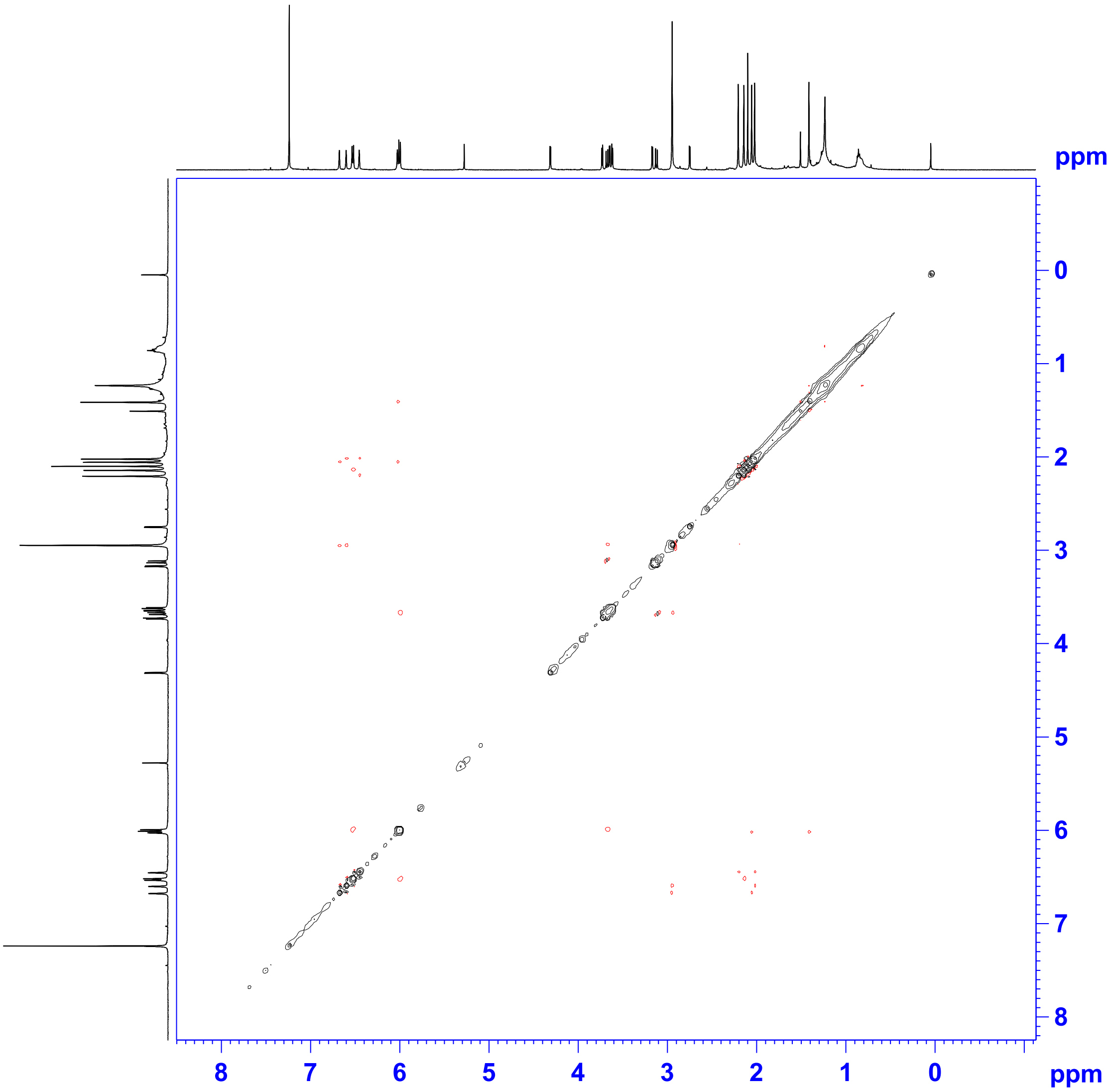

Figure S4. ^{1}H,^{1}H NOESY spectrum (500 MHz, CDCl$_3$, 300 K) of **2a**.

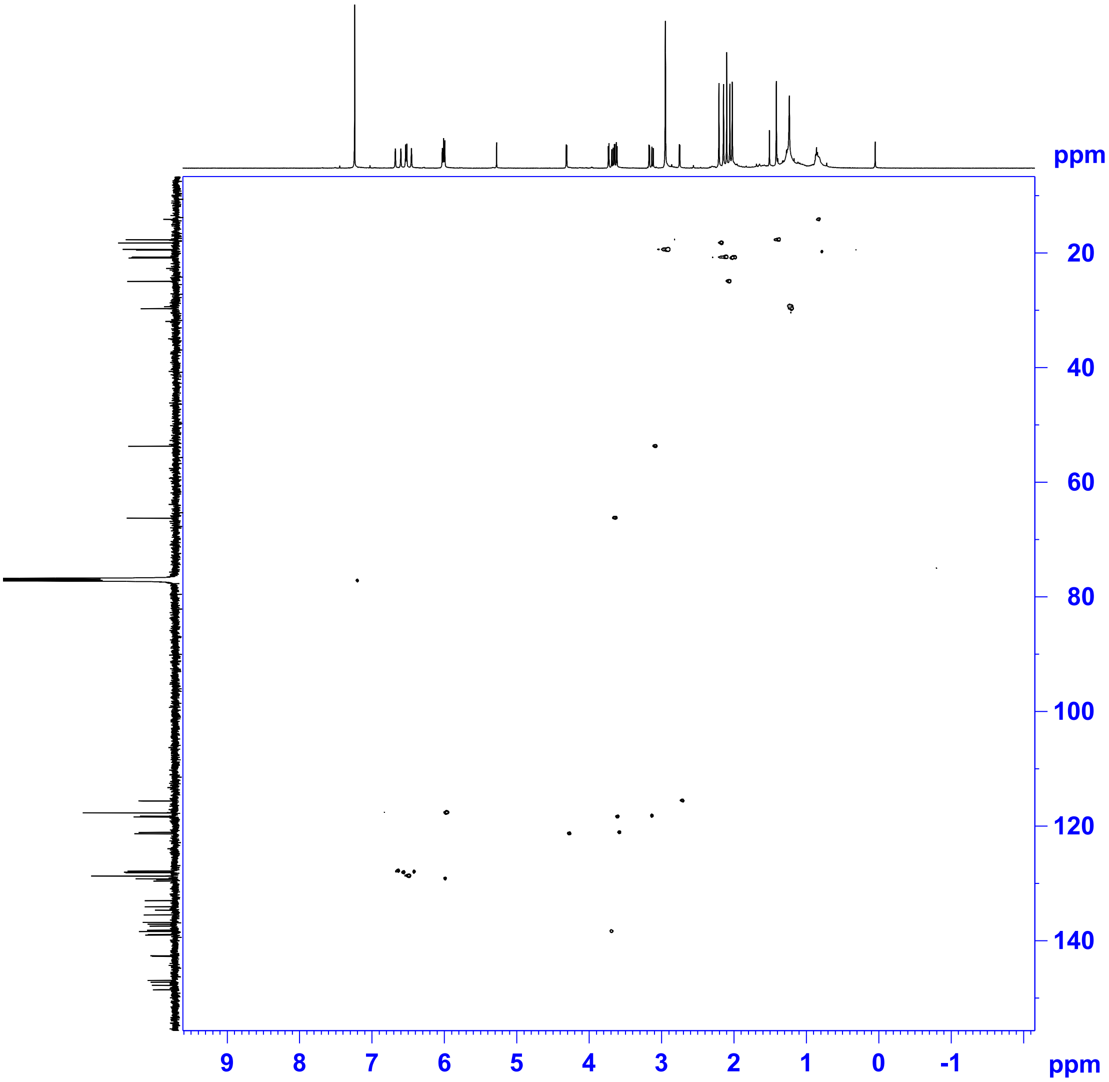

Figure S5. $^{1}H,^{13}C$ HSQC spectrum ($CDCl_3$, 300 K) of **2a**.

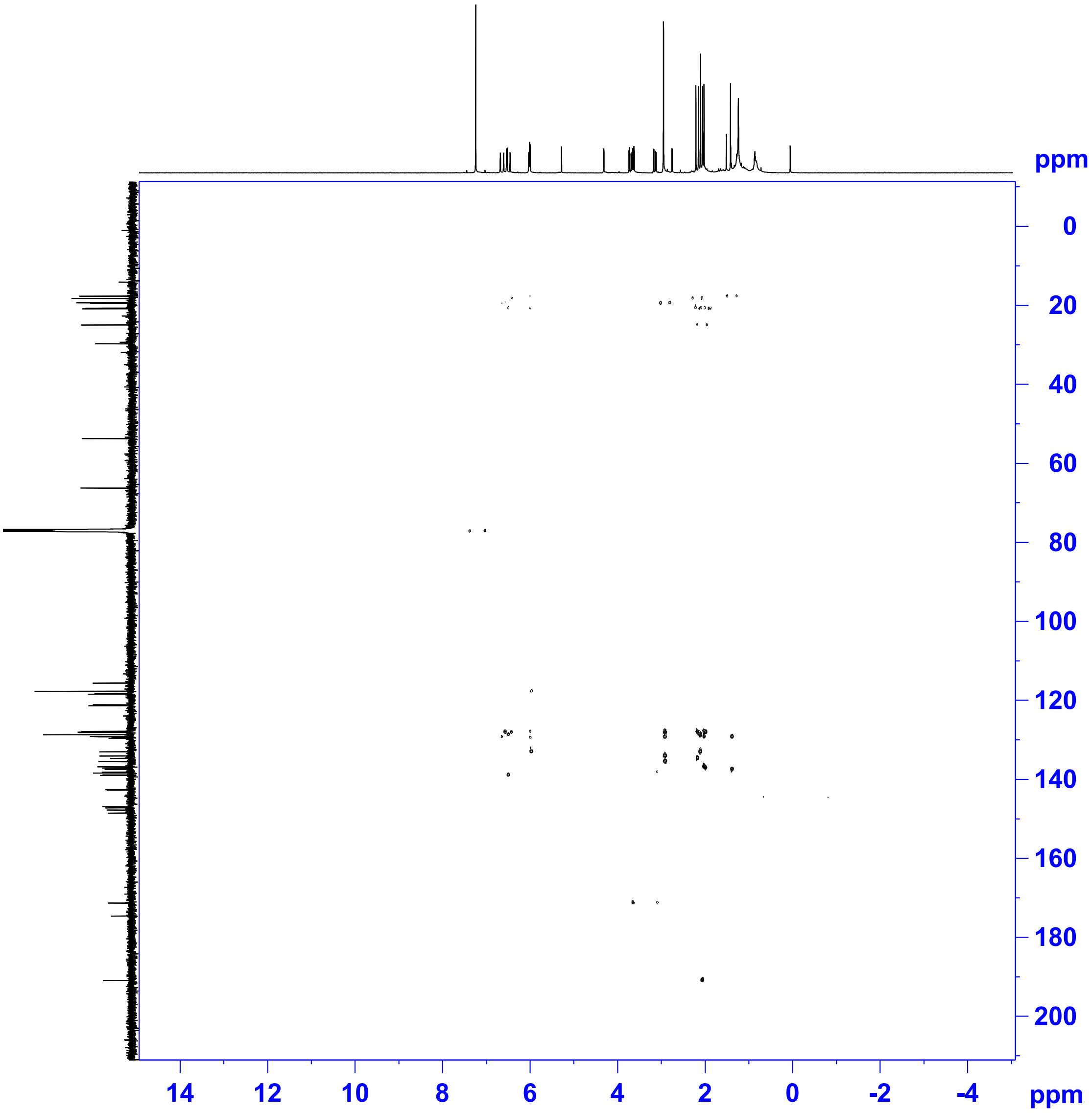

Figure S6. ^{1}H,^{13}C HMBC spectrum (CDCl$_3$, 300 K) of **2a**.

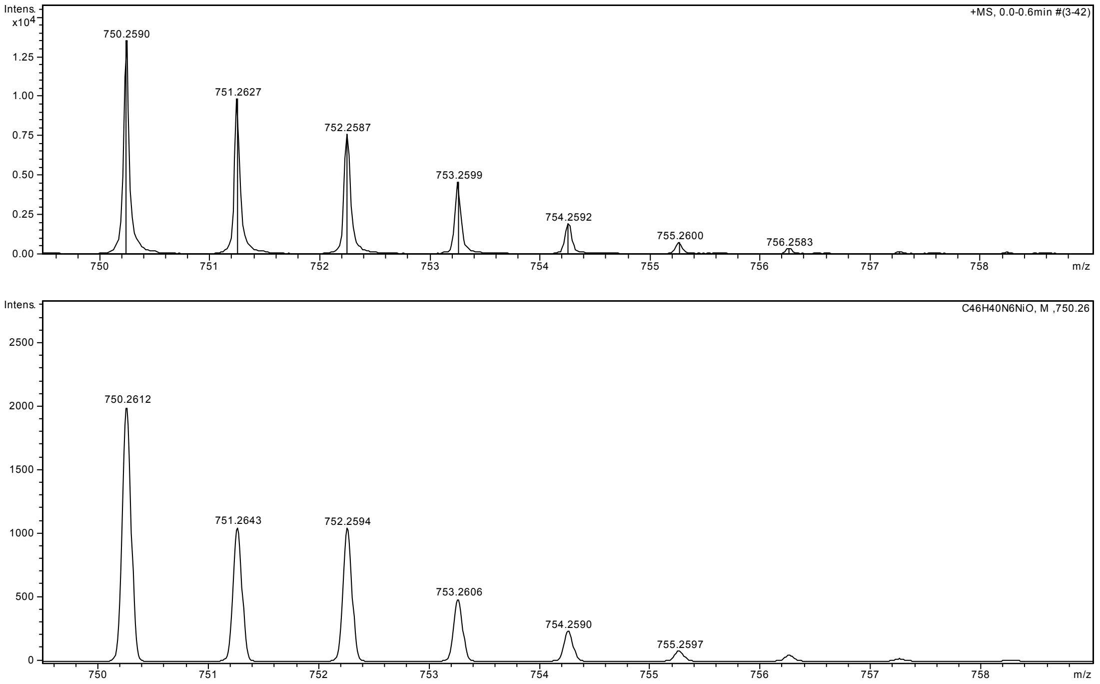

Figure S7. HRMS (ESI+ TOF) spectrum of **2a** (top) and simulated isotope pattern (bottom) for $[M^{\cdot}]^+$ molecular ion.

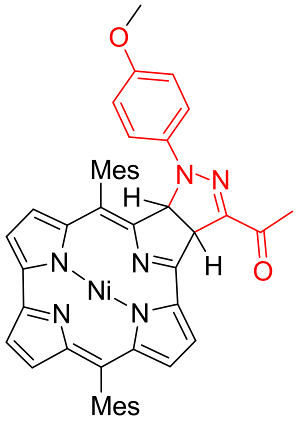

Selected data for **2b**: ^{1}H NMR (600MHz, CDCl$_3$, 298K) δ = 1.39 (s, 3H, -CH$_3$), 2.02 (s, 3H, -CH$_3$), 2.06 (s, 3H, -CH$_3$), 2.07 (s, 3H, -CH$_3$), 2.19 (s, 3H, -CH$_3$), 2.77 (d, *J* = 3.6 Hz, 1H, pyrrH), 2.95 (s, 3H, -CH$_3$), 2.96 (s, 3H, -CH$_3$), 3.15 (d, *J* = 10.2 Hz, 1H, pyrrH), 3.18 (d, *J* = 4.2 Hz, 1H, pyrrH), 3.63 (d, *J* = 4.8 Hz, 1H, pyrrH), 3.66 (s, 3H, -OCH$_3$), 3.67 (d, *J* = 3.6 Hz, 1H, pyrrH), 3.68 (d, *J* = 10.2 Hz, 1H, pyrrH), 3.74 (d, *J* = 4.8 Hz, 1H, pyrrH), 4.32 (d, *J* = 4.2 Hz, 1H, pyrrH), 6.07 (d, *J* = 9.0 Hz, 2H, ArH), 6.09 (s, 1H, ArH), 6.28 (d, *J* = 9.0 Hz, 2H, ArH), 6.45 (s, 1H, ArH), 6.61 (s, 1H, ArH), 6.69 (s, 1H, ArH); ^{13}C NMR (126MHz, CDCl$_3$, 298 K) δ_C = 17.6 (-CH$_3$), 18.2 (-CH$_3$), 19.4 (-CH$_3$), 19.6 (-CH$_3$), 20.8 (-CH$_3$), 20.9 (-CH$_3$), 24.9 (-CH$_3$), 53.7 (pyrrC), 55.4 (-OCH$_3$), 66.7 (pyrrC), 113.6, 115.7, 118.3, 118.5, 119.5, 121.1, 121.4, 127.9, 128.1, 129.3, 129.4, 129.5, 134.2, 134.6, 134.9, 135.5, 136.7, 137.1, 137.5, 137.7, 138.4, 138.7, 142.5, 142.7, 146.7, 147.1, 147.5, 148.5, 156.0, 171.1, 174.5, 190.8 (acetyl C=O). UV-vis (CH$_2$Cl$_2$) λ_{max}/nm (logε): 338 (4.57), 411 (sh), 469 (sh). ESI-HRMS calc. for [$C_{46}H_{40}N_6NiO_2$]$^+$ (M$^+$): 766.2561, Found: 766.2551.

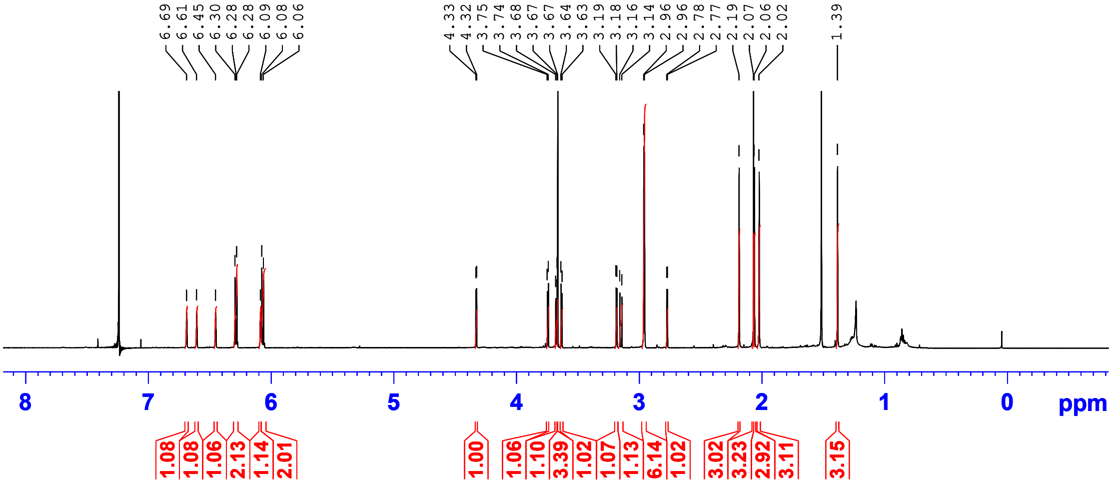

Figure S8. ^{1}H NMR spectrum (600 MHz, $CDCl_3$, 300 K) of **2b**. S – residual $CHCl_3$ signal, * - impurities.

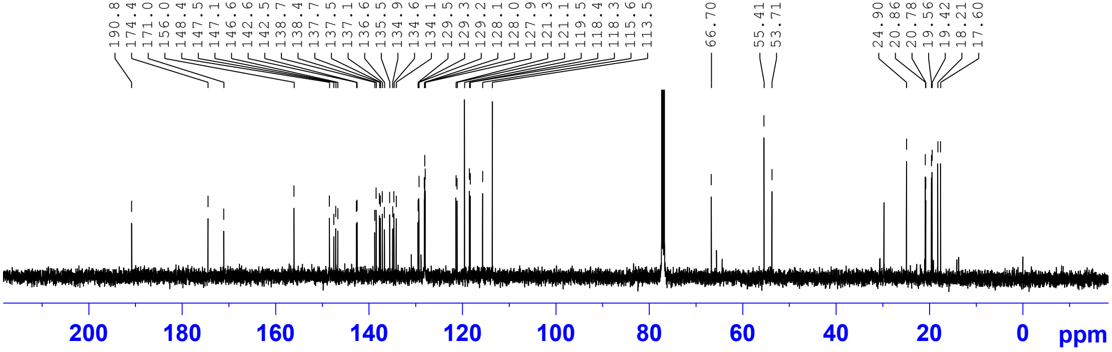

Figure S9. ^{13}C NMR spectrum (126 MHz, $CDCl_3$, 300 K) of **2b**. * - impurities.

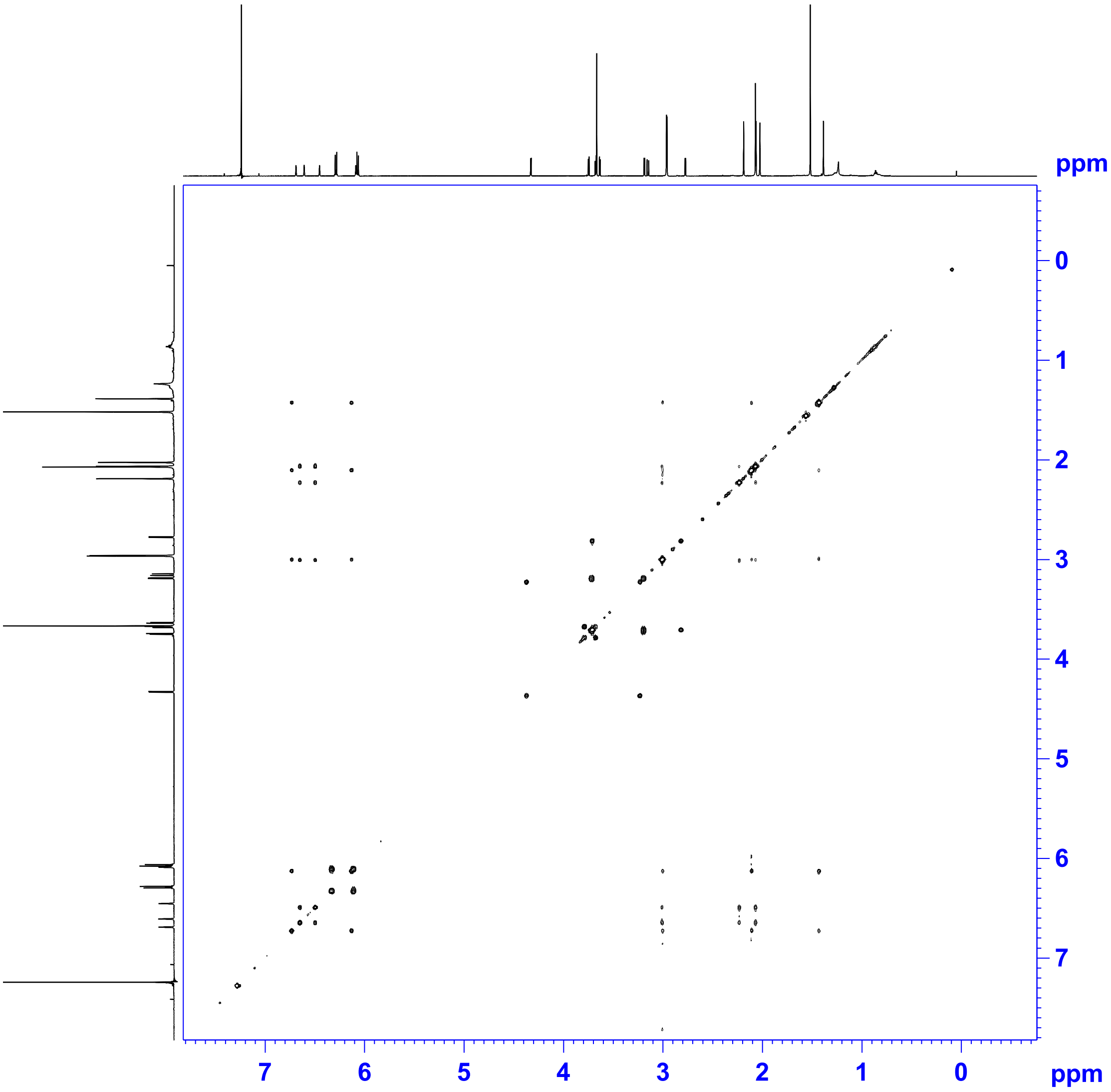

Figure S10. ^{1}H,^{1}H COSY spectrum (600 MHz, $CDCl_3$, 300 K) of **2b**.

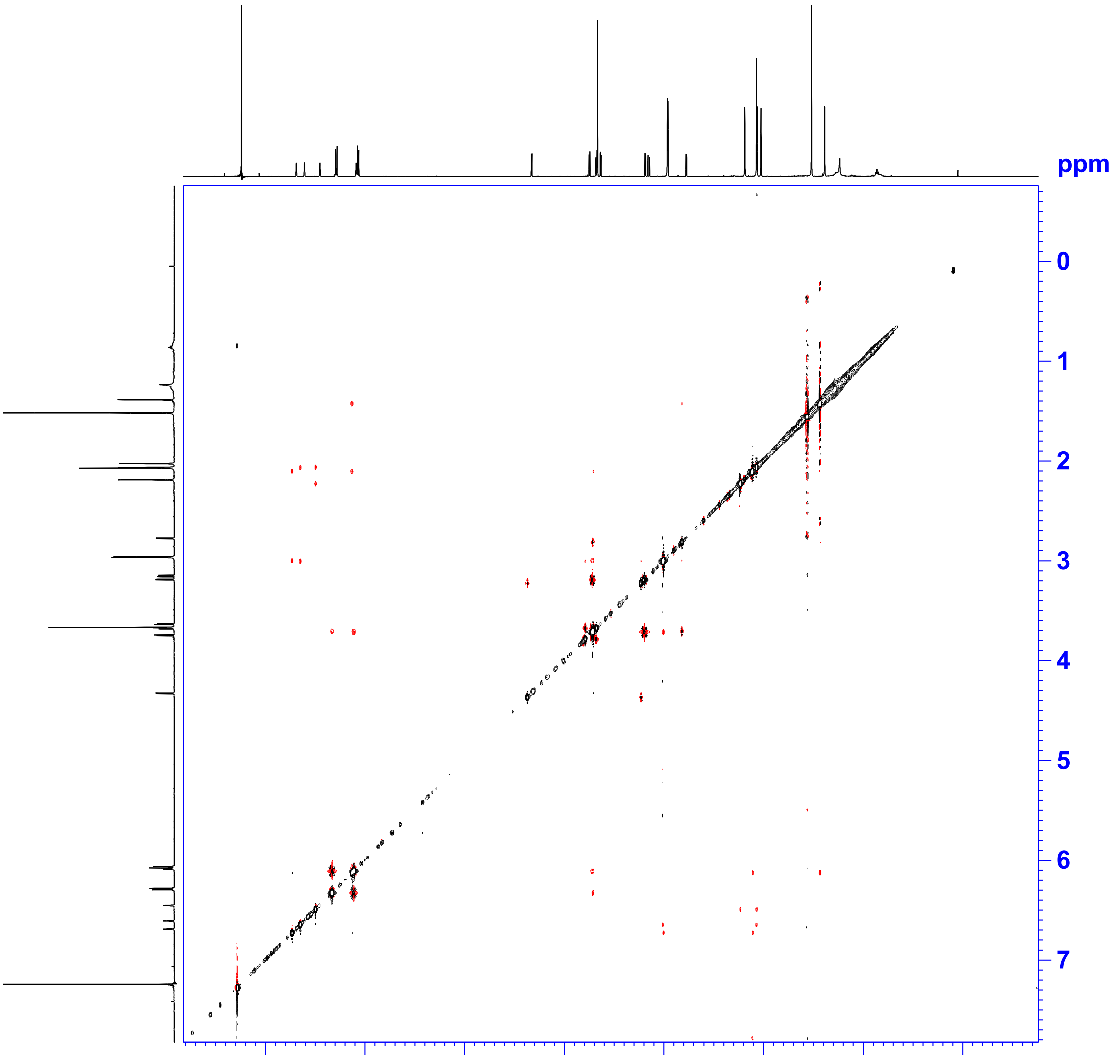

Figure S11. ^{1}H,^{1}H NOESY spectrum (600 MHz, CDCl$_3$, 300 K) of **2b**.

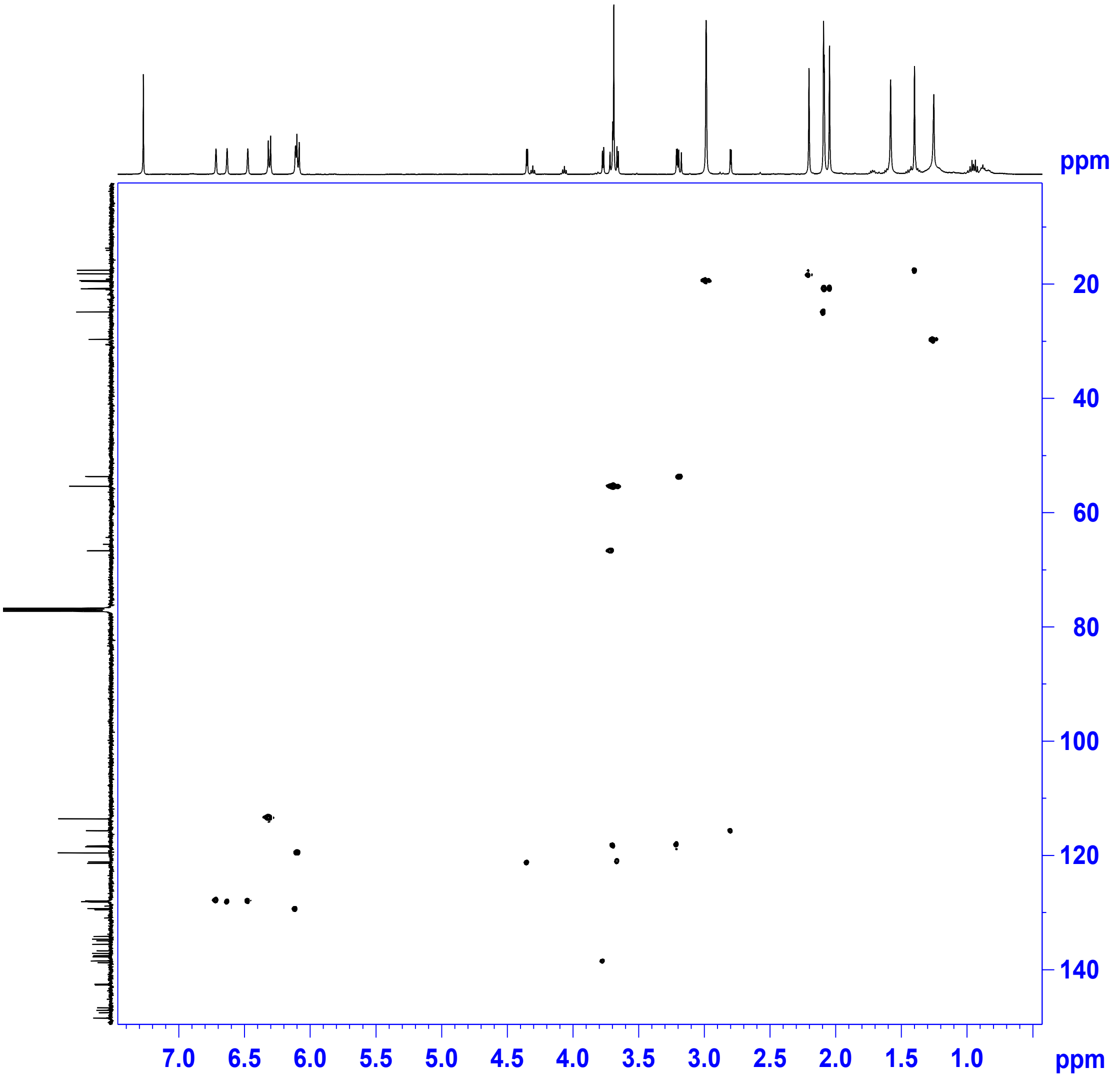

Figure S12. ^{1}H,^{13}C HSQC spectrum (CDCl$_3$, 300 K) of **2b**.

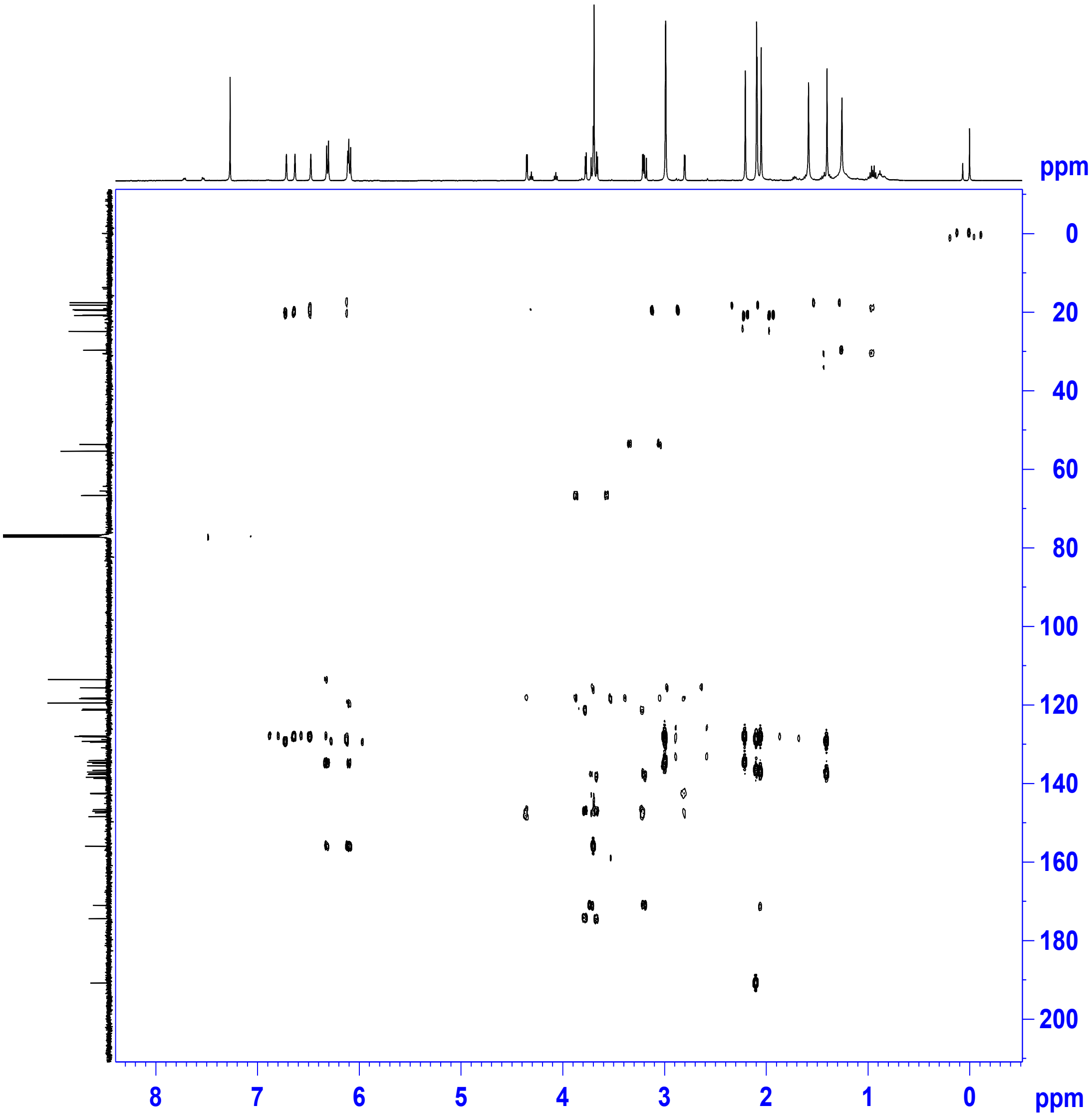

Figure S13. ^{1}H,^{13}C HMBC spectrum (CDCl$_3$, 300 K) of **2b**.

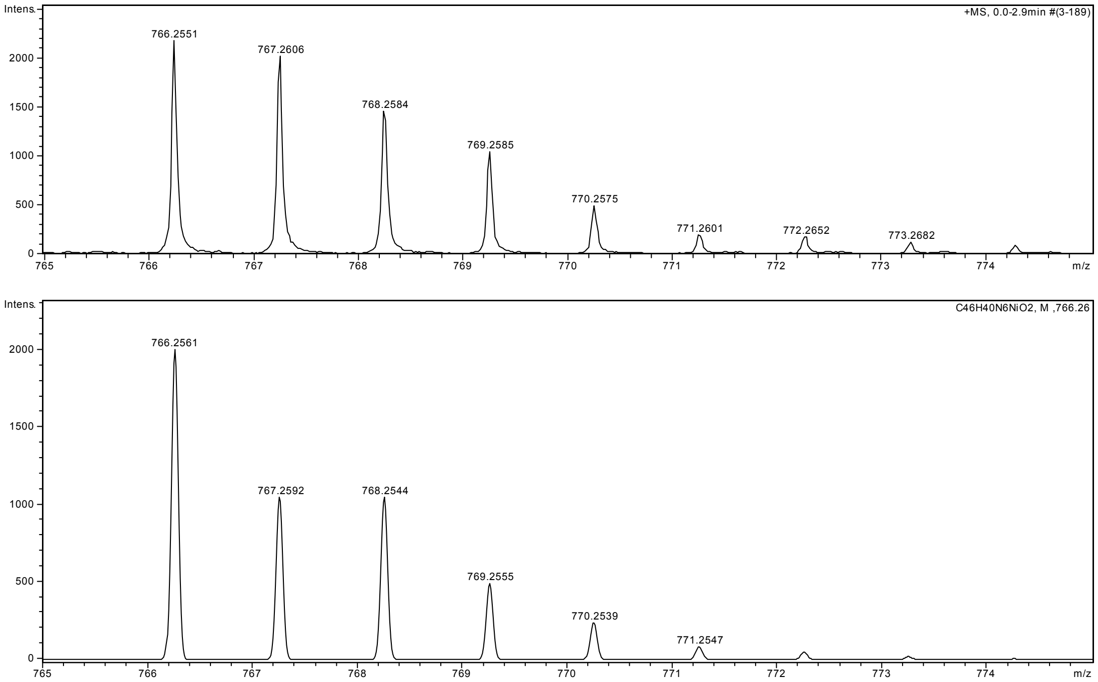

Figure S14. HRMS (ESI+ TOF) spectrum of **2b** (top) and simulated isotope pattern (bottom) for $[M^{\cdot}]^+$ molecular ion.

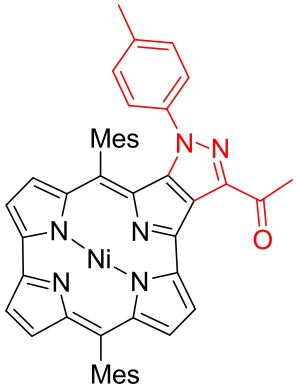

Selected data for **3a**: ^{1}H NMR (500MHz, CDCl$_3$, 298K) δ = 1.15 (d, *J* = 3.5 Hz, 1H, pyrrH), 1.54 (d, *J* = 4.0 Hz, 1H, pyrrH), 1.64 (d, *J* = 3.5 Hz, 1H, pyrrH), 1.69 (s, 3H, -CH$_3$), 1.70 (s, 3H, -CH$_3$), 1.77 (d, *J* = 4.5 Hz, 1H, pyrrH), 1.86 (s, 3H, -CH$_3$), 1.98 (d, *J* = 4.5 Hz, 1H, pyrrH), 1.99 (s, 3H, -CH$_3$), 2.47 (d, *J* = 4.0 Hz, 1H, pyrrH), 2.62 (s, 6H, -CH$_3$), 2.87 (s, 6H, -CH$_3$), 5.84 (s, 2H, ArH), 5.86 (d, *J* = 8.0 Hz, 2H, ArH), 6.30 (s, 2H, ArH), 6.35 (d, *J* = 8.0 Hz, 2H, ArH); ^{13}C NMR (125MHz, CDCl$_3$, 298 K) δ$_C$ = 17.7 (-CH$_3$), 17.8 (-CH$_3$), 20.5 (-CH$_3$), 20.6 (-CH$_3$), 20.9 (-CH$_3$), 25.2 (-CH$_3$), 113.8, 117.5, 117.6, 121.9, 122.5, 122.6, 122.64, 125.8, 126.4, 128.0, 128.2, 128.4, 132.7, 133.1, 133.6, 134.8, 135.4, 136.8, 137.2, 140.7, 147.9, 148.7, 149.2, 149.4, 150.3, 155.1, 155.2, 157.6, 165.5, 177.0, 190.9 (acetyl C=O). UV-vis (CH$_2$Cl$_2$) λ$_{max}$/nm (logε): 448 (4.41), 478 (sh), 511 (sh). ESI-HRMS calc. for [C$_{46}$H$_{38}$N$_6$NiO]$^+$ (M$^+$): 748.2455, Found: 748.2424.

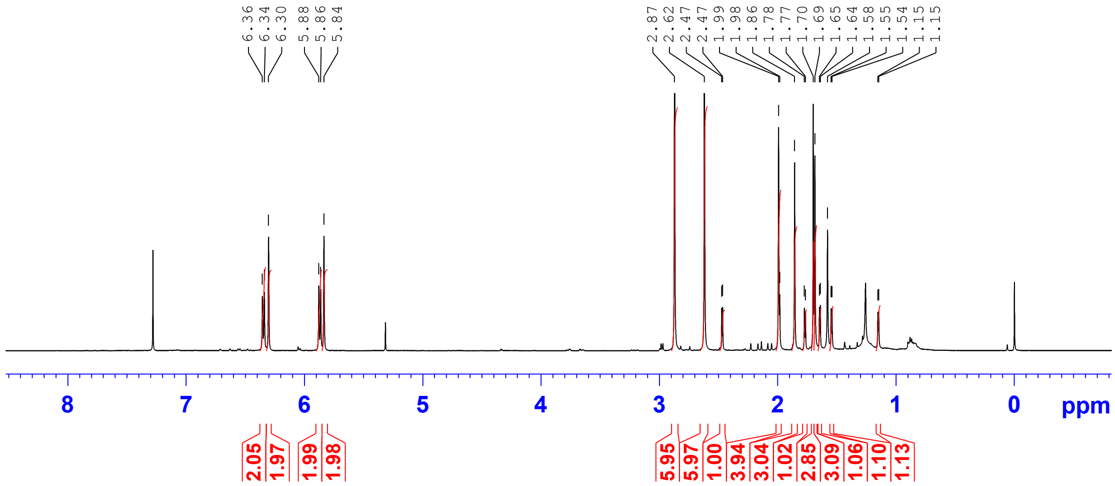

Figure S15. ^{1}H NMR spectrum (500 MHz, CDCl$_3$, 300 K) of **3a**. S – residual CHCl$_3$ signal, * - impurities.

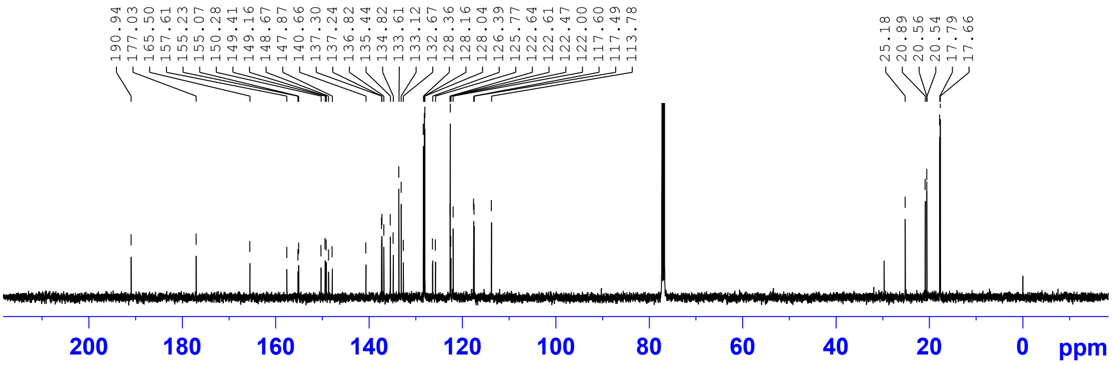

Figure S16. ^{13}C NMR spectrum (126 MHz, $CDCl_3$, 300 K) of **3a**. * - impurities.

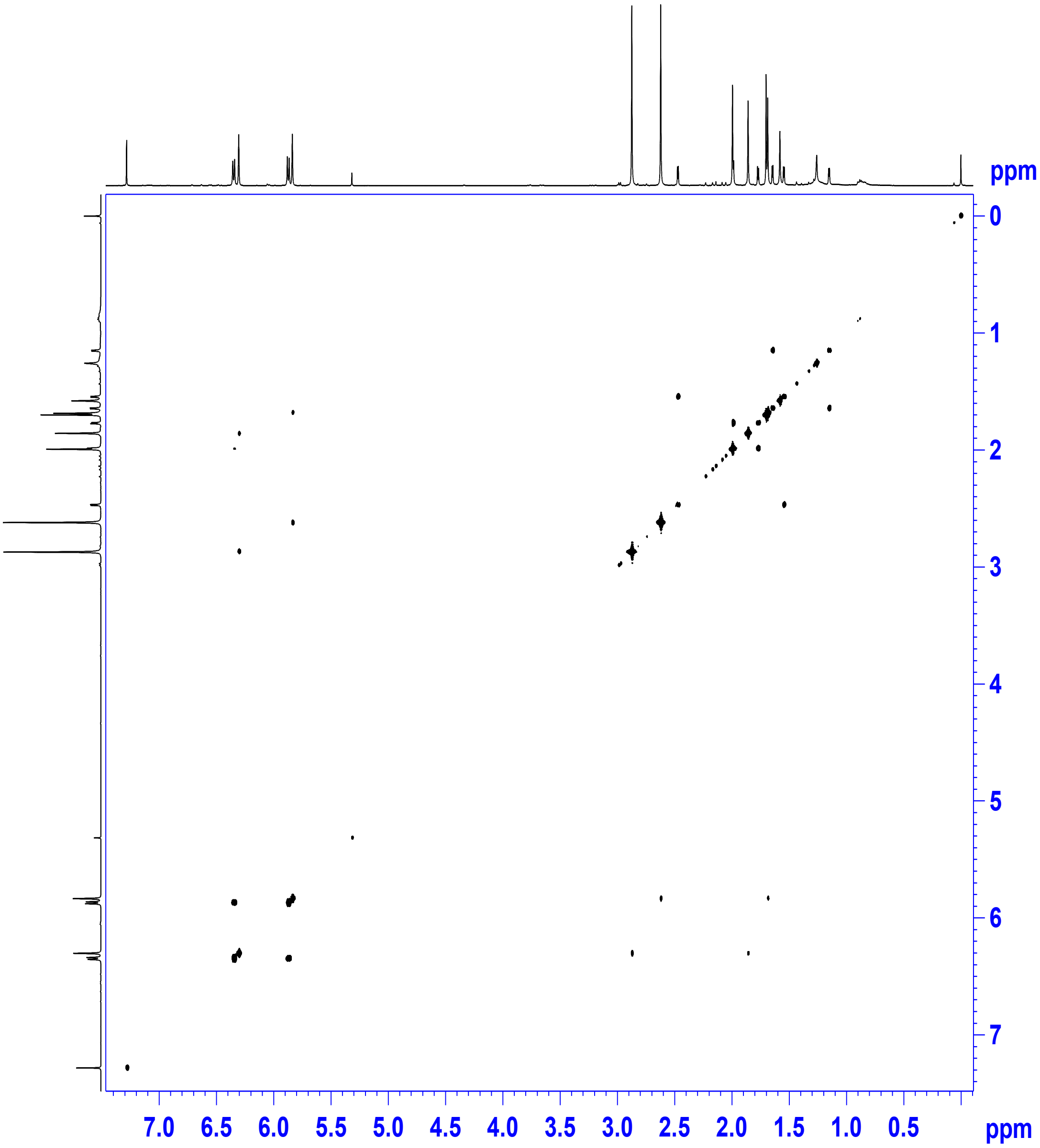

Figure S17. ^{1}H,^{1}H COSY spectrum (500 MHz, $CDCl_3$, 300 K) of **3a**.

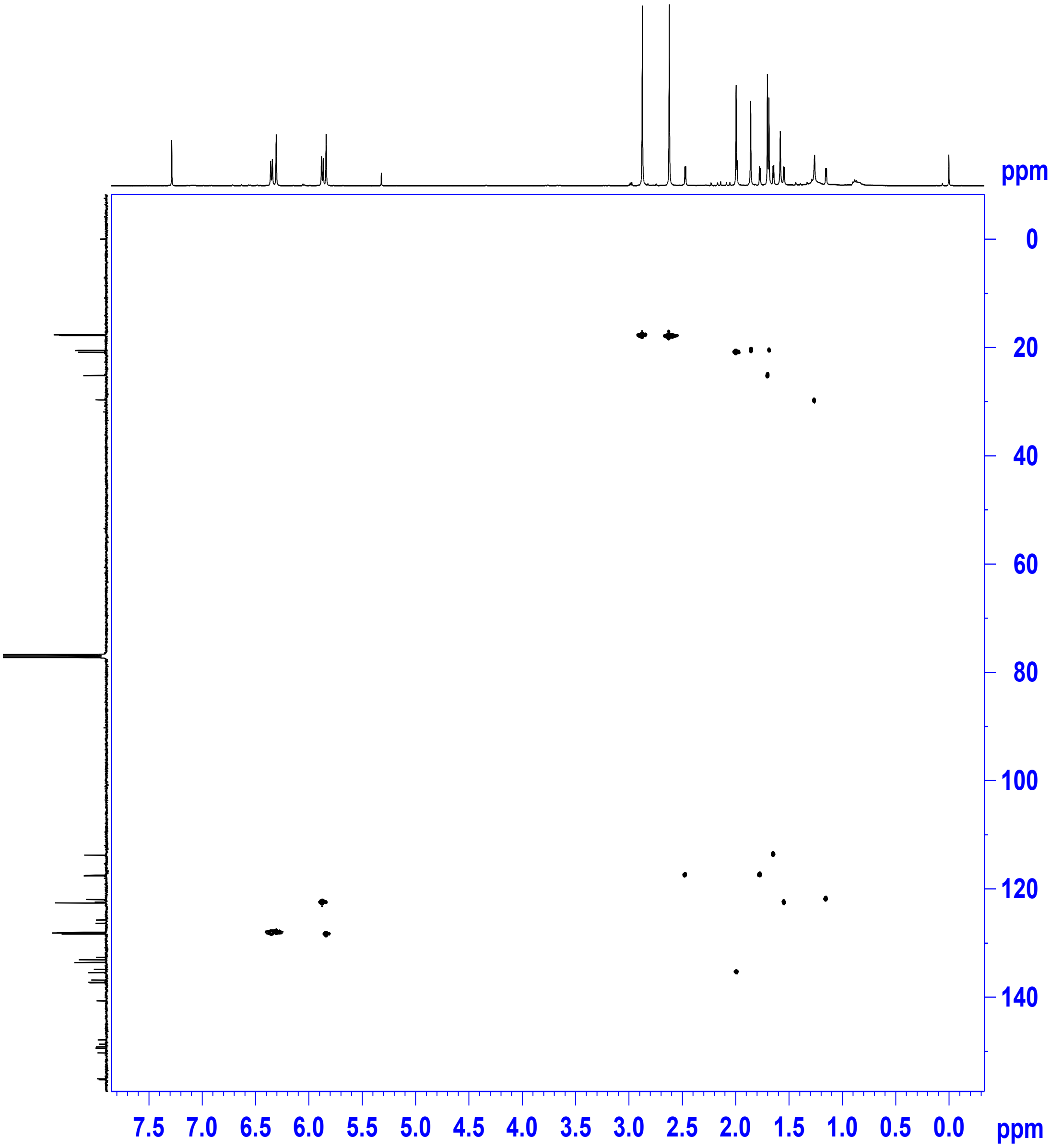

Figure S18. ^{1}H,^{13}C HSQC spectrum (CDCl$_3$, 300 K) of **3a**.

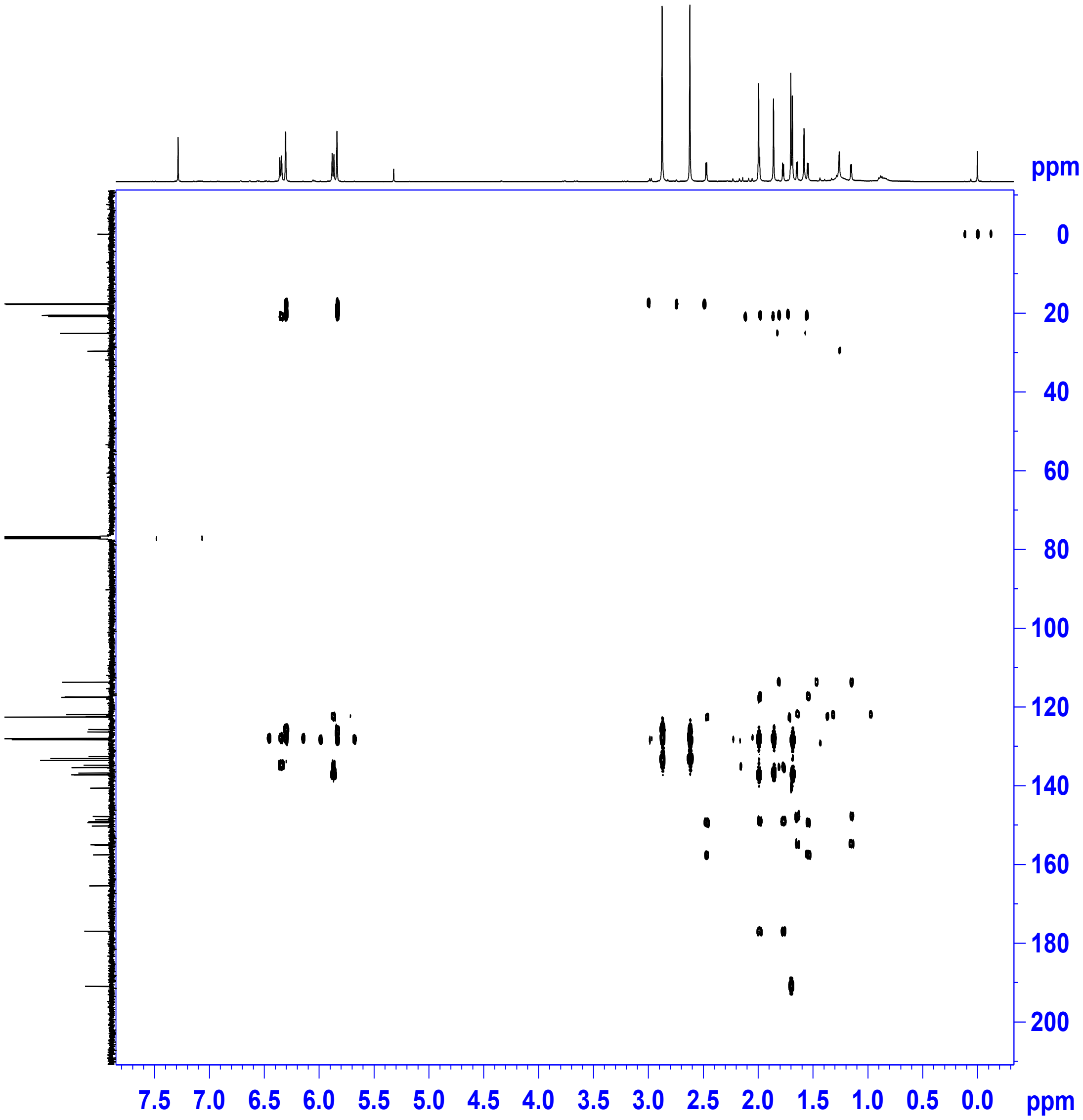

Figure S19. ^{1}H,^{13}C HMBC spectrum (CDCl$_3$, 300 K) of **3a**.

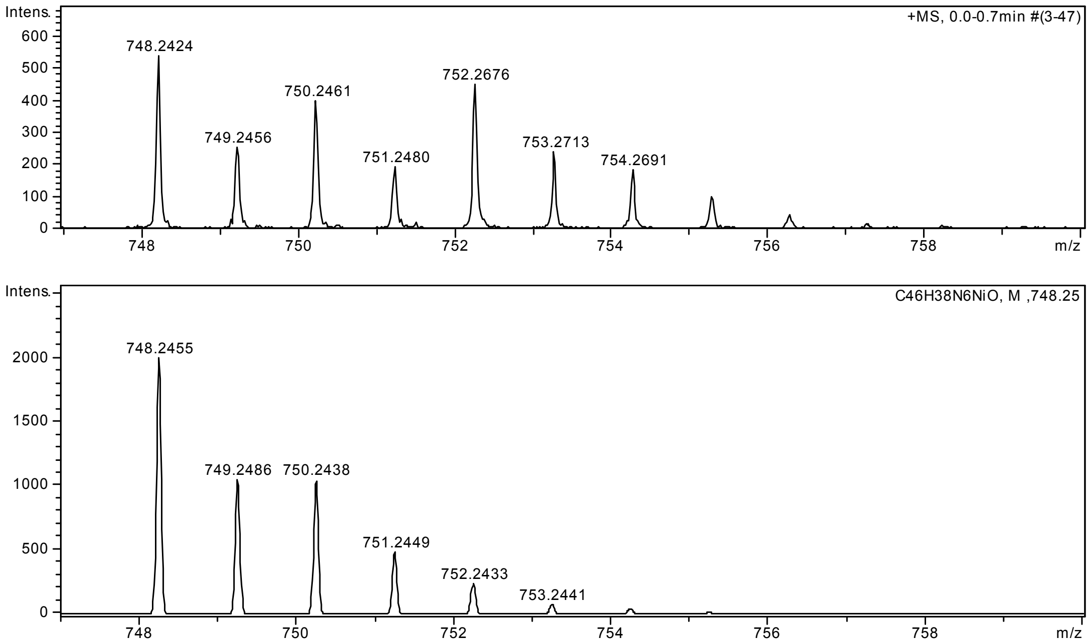

Figure S20. HRMS (ESI+ TOF) spectrum of **3a** (top) and simulated isotope pattern (bottom) for $[M]^+$ molecular ion.

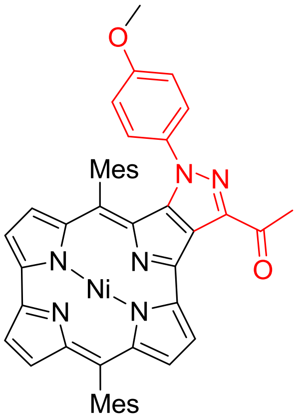

Selected data for **3b**: ^{1}H NMR (500MHz, $CDCl_3$, 298K) δ = 1.17 (d, *J* = 4.0 Hz, 1H, pyrrH), 1.54 (d, *J* = 4.0 Hz, 1H, pyrrH), 1.65 (d, *J* = 4.0 Hz, 1H, pyrrH), 1.69 (s, 6H, -CH_3), 1.77 (d, *J* = 4.5 Hz, 1H, pyrrH), 1.86 (s, 3H, -CH_3), 1.99 (d, *J* = 4.5 Hz, 1H, pyrrH), 2.46 (d, *J* = 4.0 Hz, 1H, pyrrH), 2.65 (s, 6H, -CH_3), 2.86 (s, 6H, -CH_3), 3.53 (s, 3H, -OCH_3), 5.86 (s, 2H, ArH), 6.04 (d, *J* = 9.5 Hz, 2H, ArH), 6.07 (d, *J* = 9.5 Hz, 2H, ArH), 6.30 (s, 2H, ArH); ^{13}C NMR (126MHz, $CDCl_3$, 298 K) δ_C = 17.7 (-CH_3), 17.9 (-CH_3), 20.2 (-CH_3), 20.6 (-CH_3), 25.2 (-CH_3), 55.0 (-OCH_3), 112.9, 113.8, 114.9, 115.9, 117.5, 117.6, 121.9, 122.4, 122.6, 124.1, 125.8, 126.3, 128.0, 128.6, 130.4, 132.7, 133.2, 133.6, 135.5, 136.8, 137.3, 140.6, 147.9, 148.5, 149.1, 150.5, 154.9, 155.1, 157.6, 158.6, 165.5, 177.0, 190.9 (acetyl). UV-vis (CH_2Cl_2) λ_{max}/nm (logε): 444 (4.31), 477 (sh), 513 (sh). ESI-HRMS calc. for $[C_{46}H_{38}N_6NiO_2]^+$ (M^+): 764.2404, Found: 764.2404.

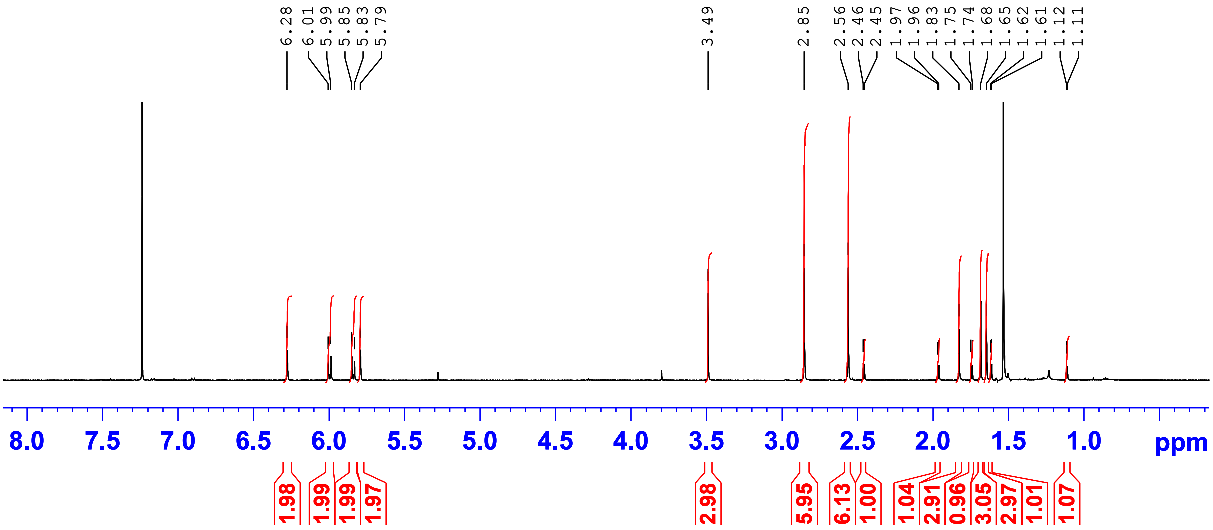

Figure S21. ^{1}H NMR spectrum (500 MHz, $CDCl_3$, 300 K) of **3b**. S – residual $CHCl_3$ signal, * - impurities.

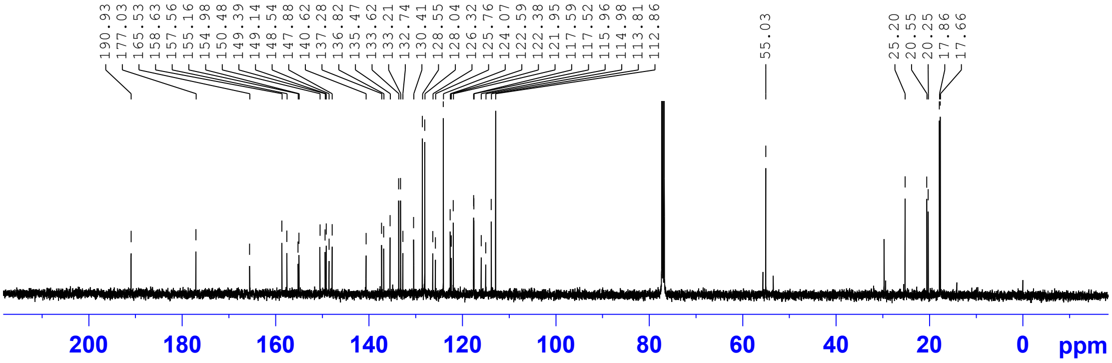

Figure S22. ^{13}C NMR spectrum (126 MHz, CDCl$_3$, 300 K) of **3b**. * - impurities.

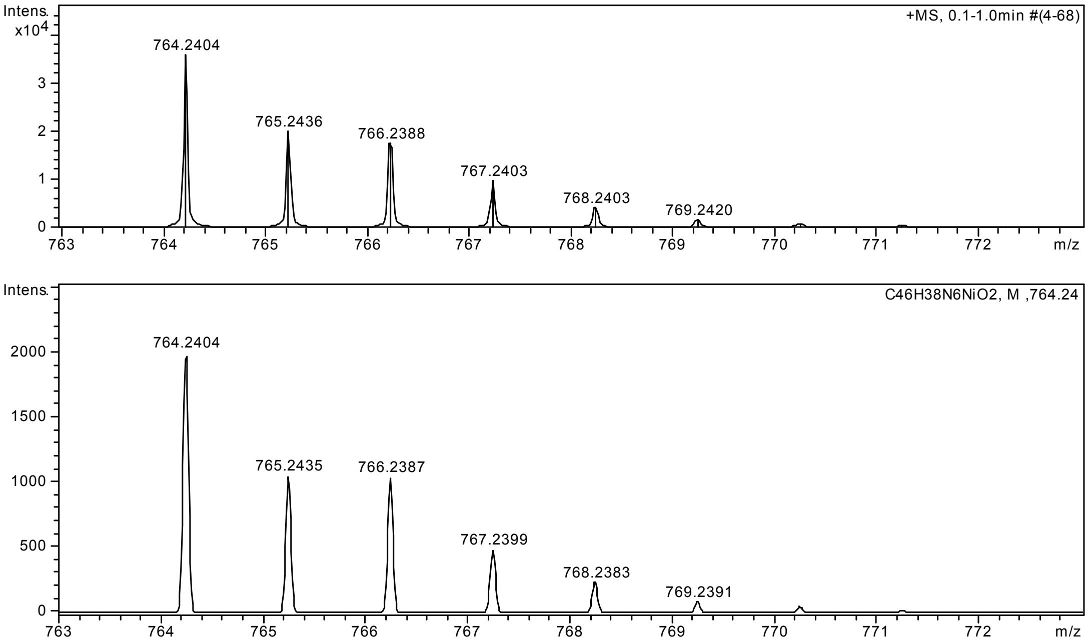

Figure S23. HRMS (ESI+ TOF) spectrum of **3b** (top) and simulated isotope pattern (bottom) for $[M^{\cdot}]^+$ molecular ion.

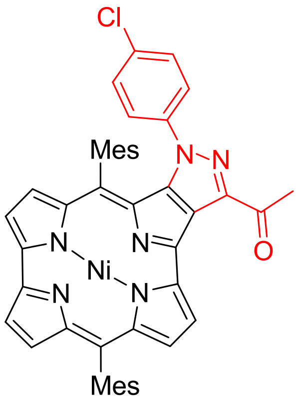

Selected data for **3c**: ^{1}H NMR (500MHz, $CDCl_3$, 298K) δ = 1.22 (d, J = 3.5 Hz, 1H, pyrrH), 1.41 (d, J = 4.0 Hz, 1H, pyrrH), 1.61 (d, J = 3.5 Hz, 1H, pyrrH), 1.64 (s, 3H, -CH_3), 1.68 (d, J = 4.5 Hz, 1H, pyrrH), 1.83 (s, 3H, -CH_3), 1.84 (s, 3H, -CH_3), 1.87 (d, J = 4.5 Hz, 1H, pyrrH), 2.30 (d, J = 4.0 Hz, 1H, pyrrH), 2.83 (s, 6H, -CH_3), 2.87 (s, 6H, -CH_3), 6.00 (s, 2H, ArH), 6.27 (s, 2H, ArH), 6.50 (d, J = 8.5 Hz, 2H, ArH), 6.64 (d, J = 8.5 Hz, 2H, ArH); ^{13}C NMR (126 MHz, $CDCl_3$, 298 K) δ_C = 17.5 (-CH_3), 17.9 (-CH_3), 20.5 (-CH_3), 20.6 (-CH_3), 25.1 (-CH_3), 113.9, 117.3, 117.6, 122.7, 122.8, 123.1, 124.3, 125.6, 126.5, 127.8, 128.0, 128.7, 133.0, 133.2, 133.4, 133.5, 135.4, 136.0, 136.8, 138.3, 141.2, 147.9, 149.2, 149.3, 149.5, 150.5, 155.6, 155.7, 157.8, 165.4, 176.9, 190.7 (acetyl). UV-vis (CH_2Cl_2) λ_{max}/nm (logε): 447 (4.57), 474 (sh), 512 (sh). ESI-HRMS calc. for $[C_{45}H_{35}ClN_6NiO]^+$ (M^+): 768.1909, Found: 768.1883.

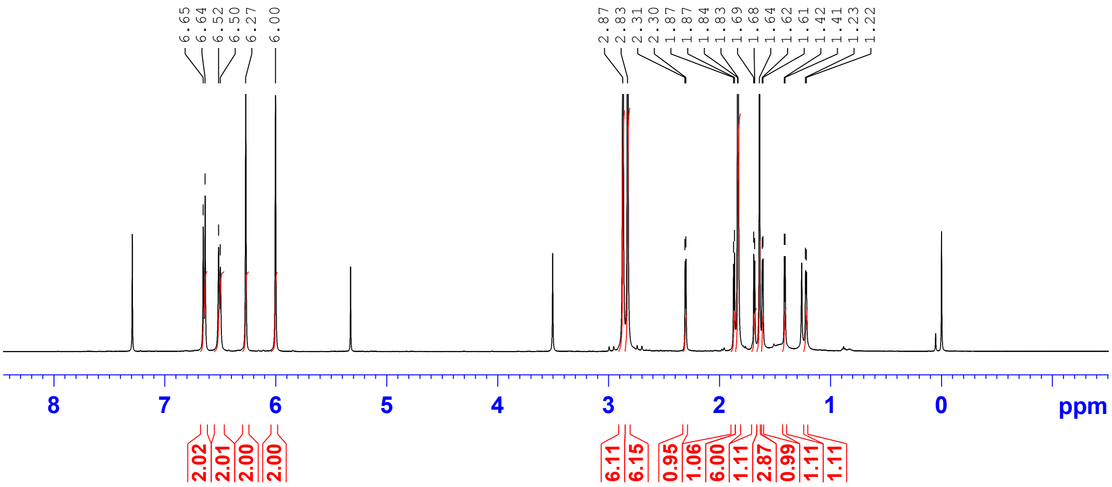

Figure S24. ^{1}H NMR spectrum (500 MHz, $CDCl_3$, 298 K) of **3c**. S – residual $CHCl_3$ signal, * - impurities.

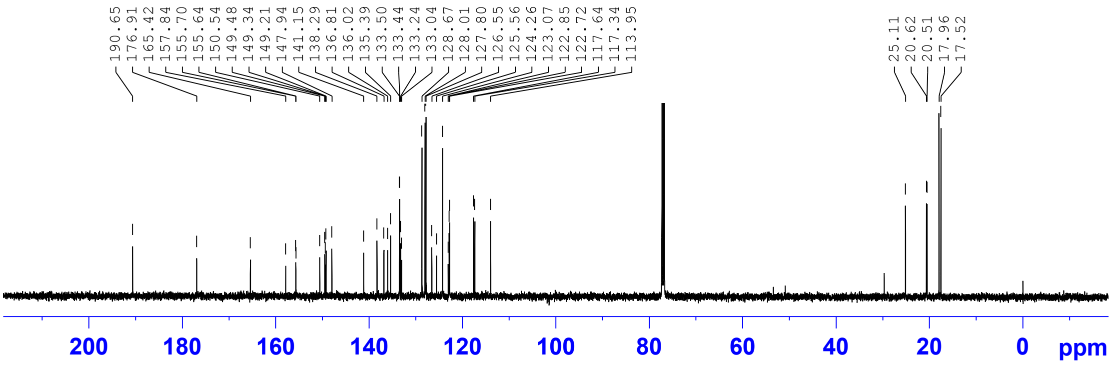

Figure S25. ^{13}C NMR spectrum (126 MHz, CDCl$_3$, 298 K) of **3c**. * - impurities.

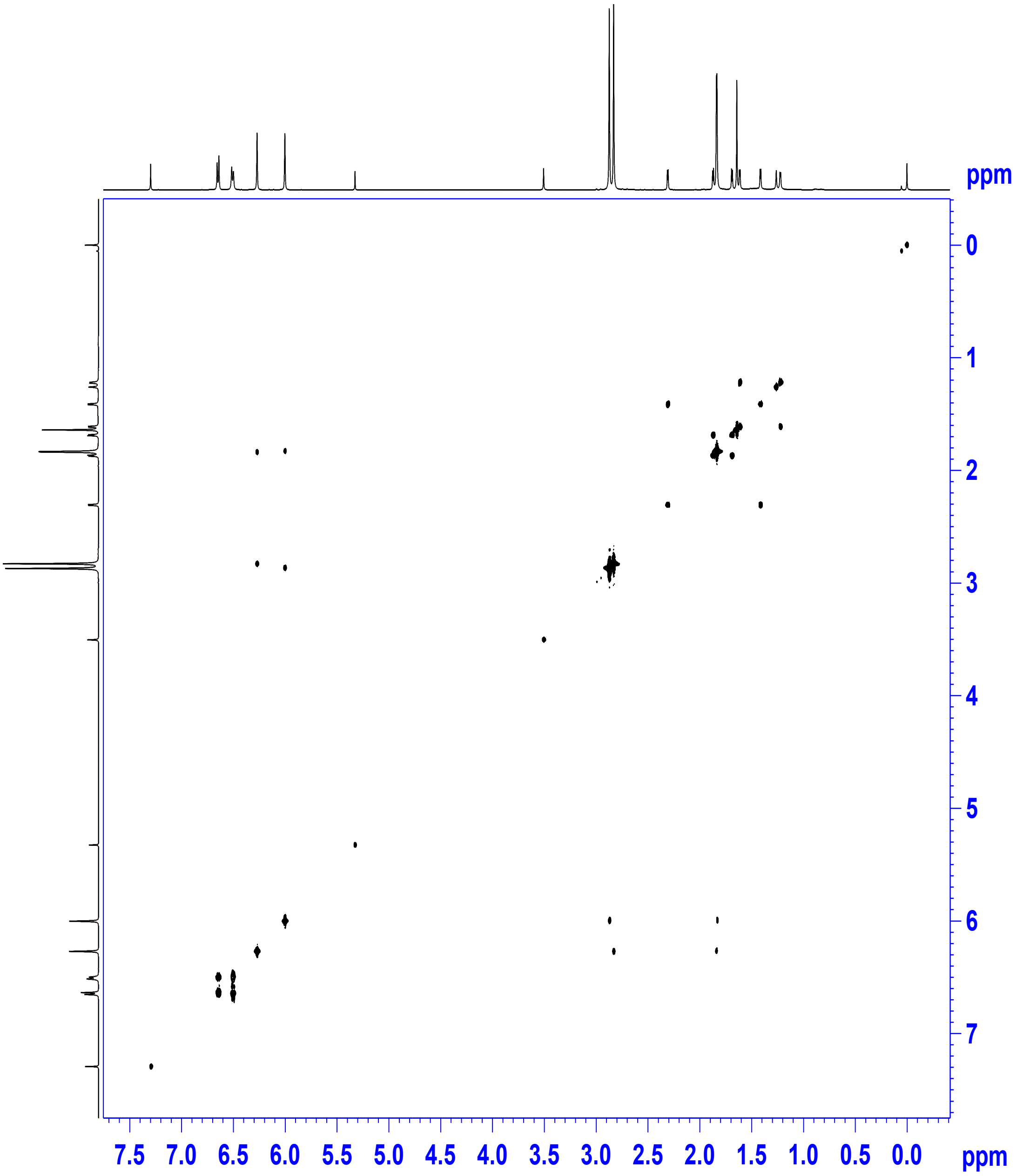

Figure S26. ^{1}H,^{1}H COSY spectrum (500 MHz, CDCl$_3$, 300 K) of **3c**.

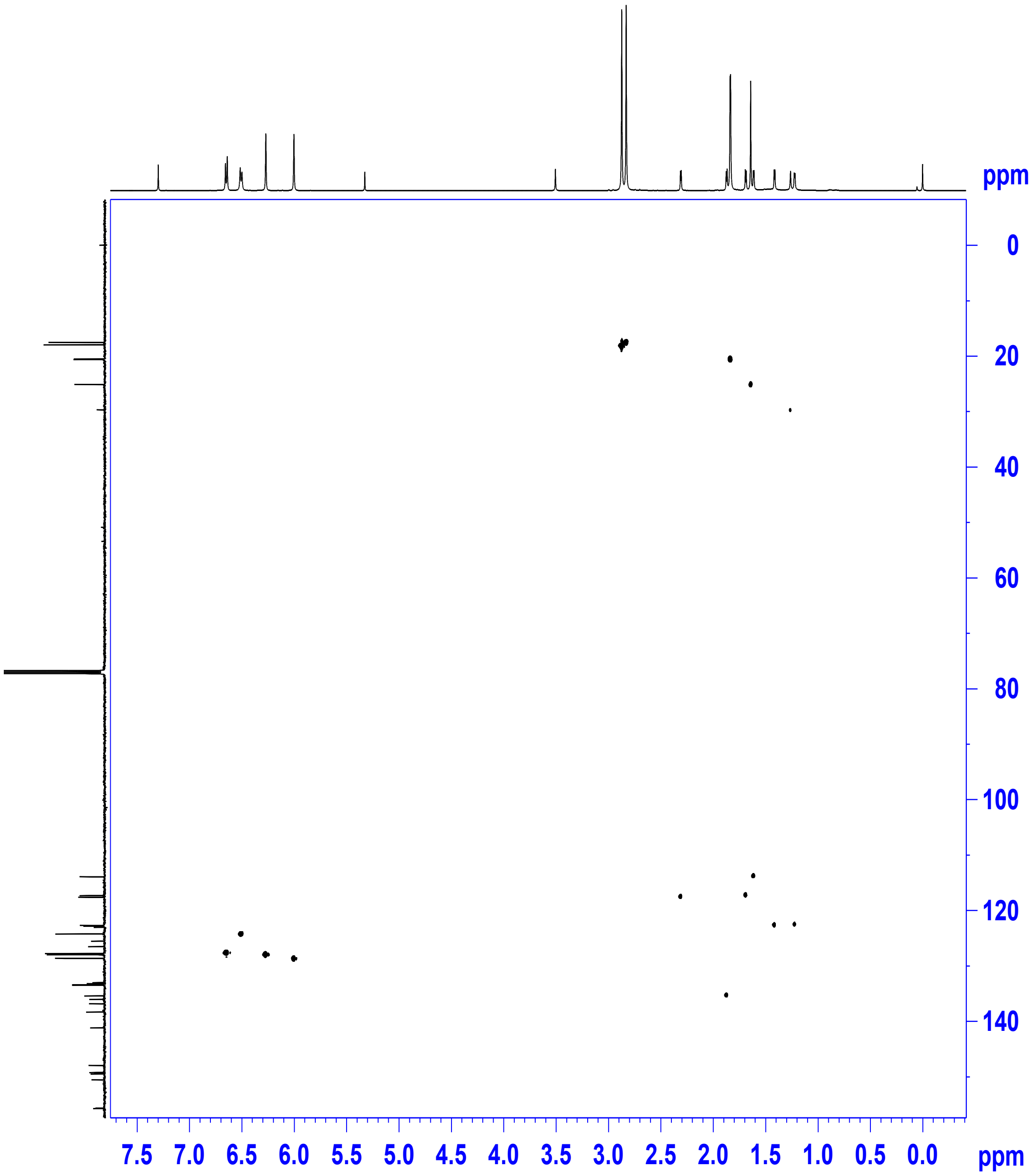

Figure S27. ^{1}H,^{13}C HSQC spectrum (CDCl$_3$, 300 K) of **3c**.

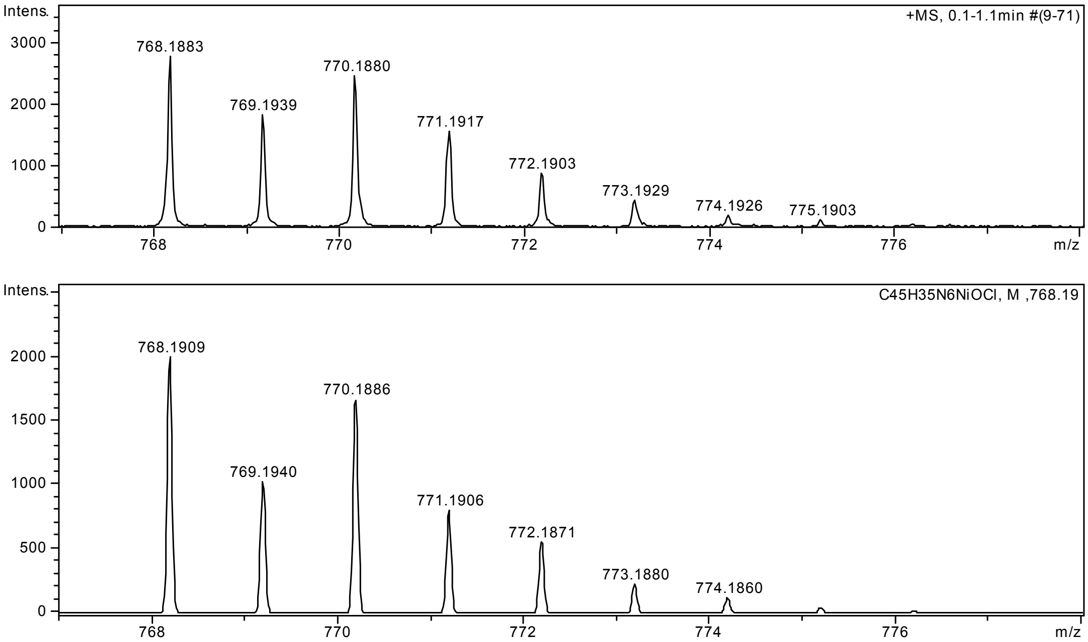

Figure S28. HRMS (ESI+ TOF) spectrum of **3c** (top) and simulated isotope pattern (bottom) for $[M]^+$ molecular ion.

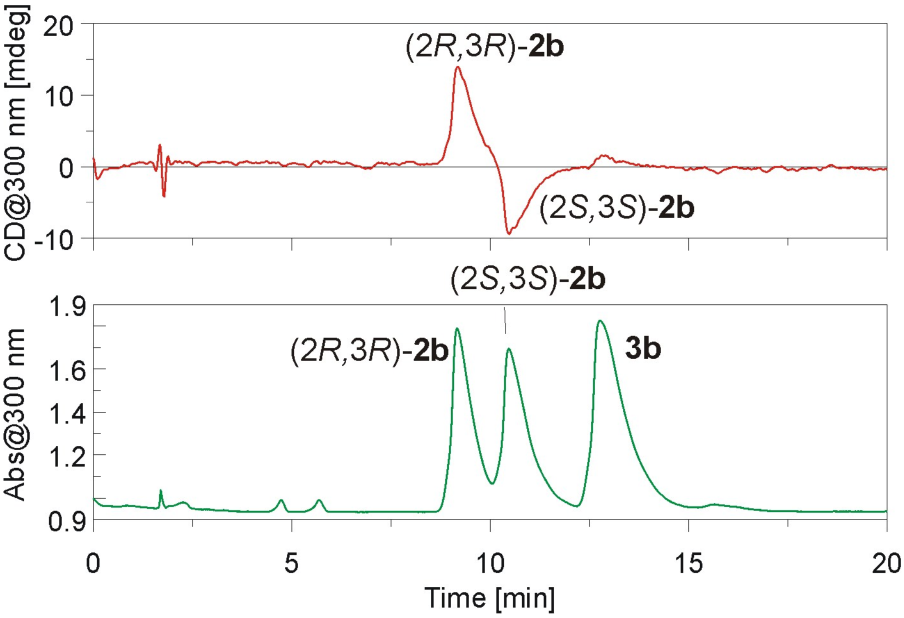

Figure S29. Chiral stationary phase (Chirex® 3010) HPLC profile (mobile phase DCM/hexane 40/60 v/v) of **2b** recorded with UV-vis absorbance detection (green trace) and CD detection (red trace) at 300 nm. Note the appearance of achiral oxidation product **3b** upon profile evolution.

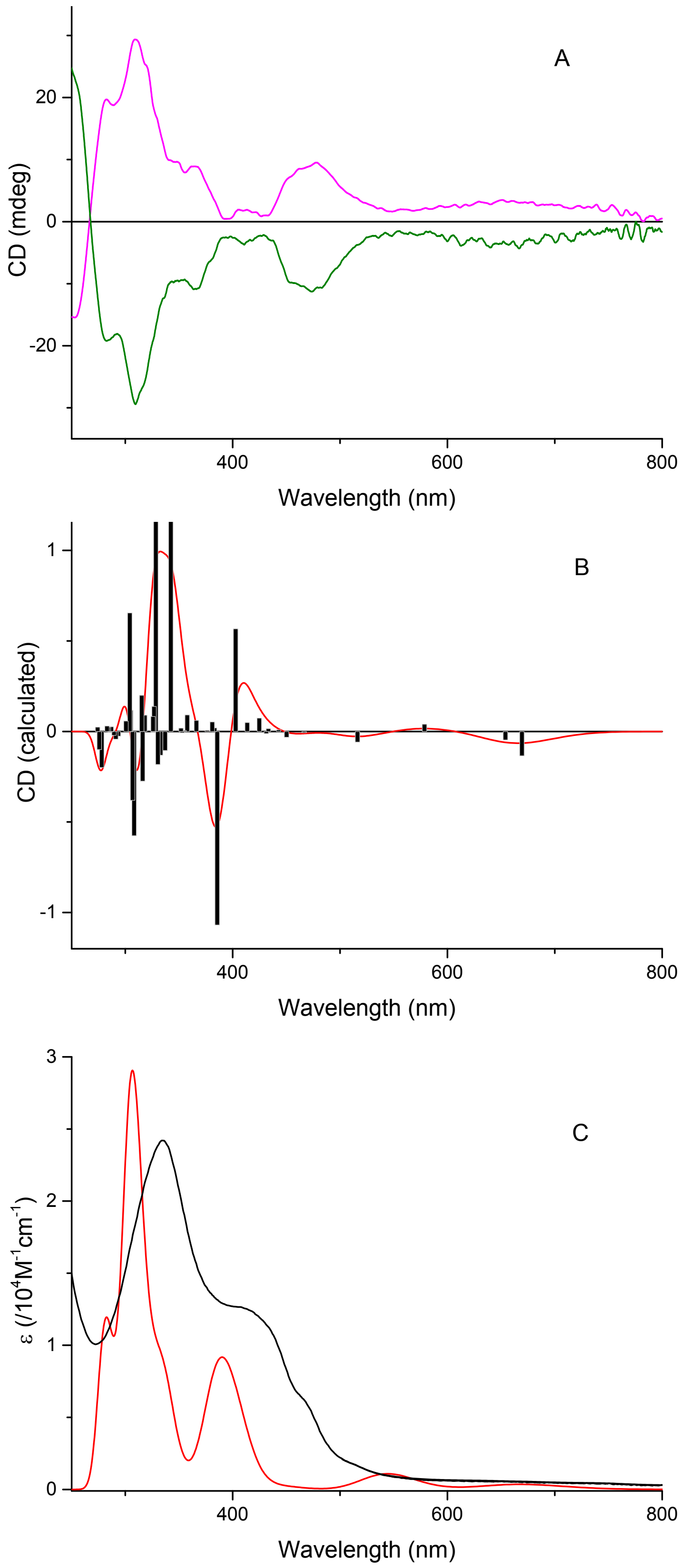

Figure S30. (A) CD spectra of enantiomers of **2b** (DCM/hexane 40/60 v/v, 298 K). (B) TDDFT simulated CD spectrum of *S,S*-**2b** (red trace) and histogram of calculated electronic transitions (black sticks). (C) Experimental (black trace) and TDDFT calculated (red trace) UV-vis spectra of *S,S*-**2b**.

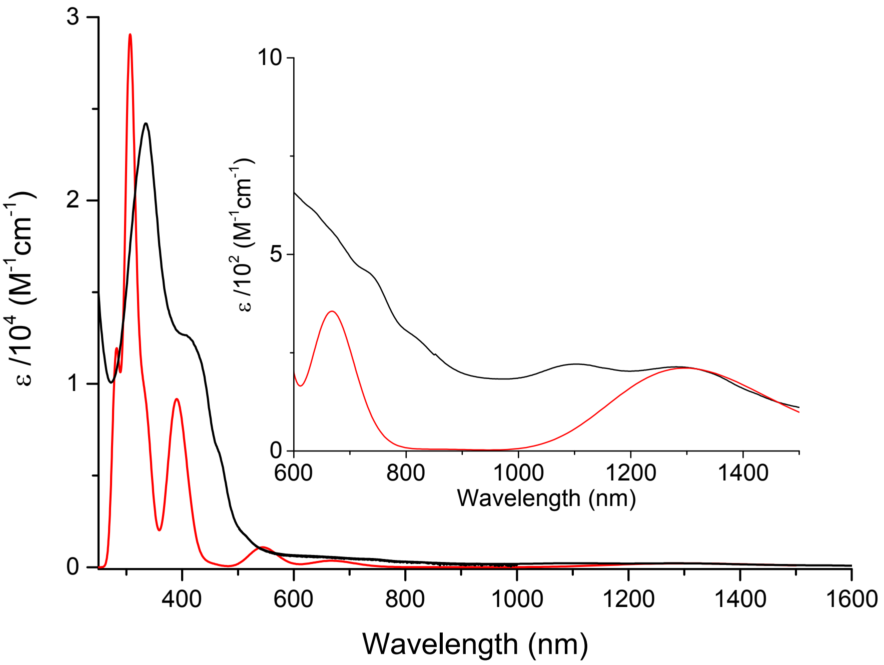

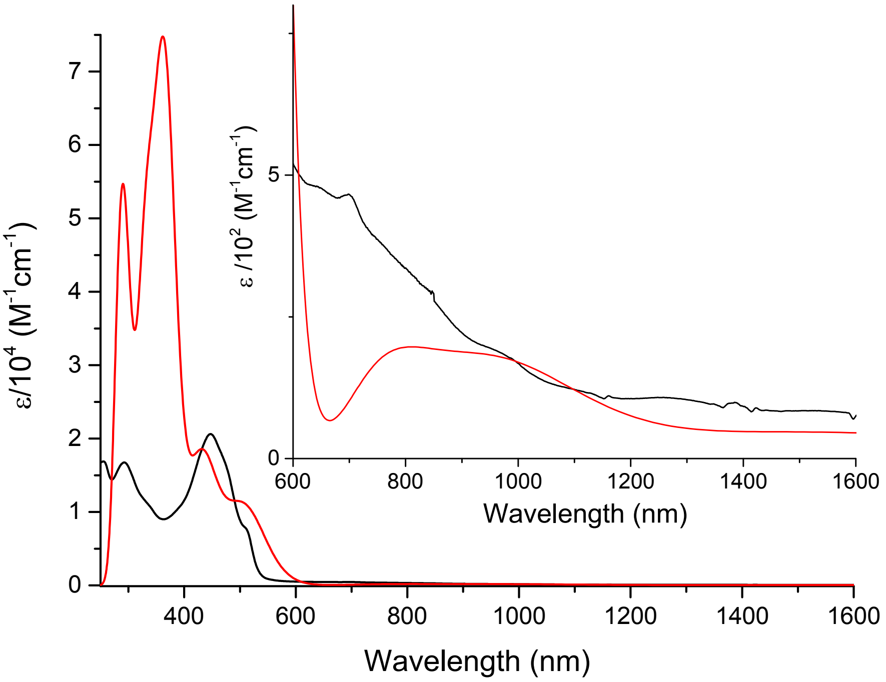

Figure S31. Experimental (black traces) and TDDFT calculated (red traces) electronic spectra of **2a** (top) and **3a** (bottom).

Table S1. TD-DFT Calculated Electronic Transitions for **2a**.

HOMO is 197

No.	Energy (cm^{-1})	Wavelength (nm)	Osc. Strength	Major contribs	Minor contribs
1	7756.63394369	1289.21901853	0.0102	HOMO->LUMO (97%)	
2	11691.0064484	855.35835124	0.0001	H-1->LUMO (98%)	
3	14939.8076884	669.352658923	0.0131	H-4->LUMO (11%), H-3->LUMO (80%)	H-2->LUMO (4%)
4	15290.658865	653.994055345	0.0039	H-4->LUMO (88%), H-3->LUMO (10%)	
5	17281.2351958	578.662340205	0.043	H-2->LUMO (95%)	H-3->LUMO (4%)
6	19370.2111669	516.256633129	0.0078	HOMO->L+1 (98%)	
7	21434.1839507	466.544470413	0.0004	H-7->LUMO (14%), H-6->LUMO (81%)	H-5->LUMO (4%)
8	22214.1220835	450.16408762	0.0069	H-5->LUMO (91%)	H-7->LUMO (6%)
9	22587.5567841	442.721631895	0.0009	H-8->LUMO (99%)	
10	23077.1353225	433.329347869	0.0003	H-7->LUMO (78%), H-6->LUMO (17%)	H-5->LUMO (4%)
11	23186.8267249	431.279369042	0.0007	H-1->L+1 (20%), H-1->L+6 (47%)	H-15->L+6 (6%), H-1->L+7 (6%), H-1->L+10 (7%)
12	23540.9041192	424.792520685	0.002	H-9->LUMO (76%)	H-10->LUMO (9%), HOMO->L+2 (8%)
13	24182.9214447	413.514968523	0.0026	H-1->L+1 (72%), H-1->L+6 (10%)	H-1->L+2 (7%)
14	24832.1977601	402.702978473	0.1874	H-13->LUMO (18%), HOMO->L+2 (63%)	H-9->LUMO (5%)
15	25933.1445556	385.606920077	0.2353	H-10->LUMO (54%), H-3->L+6 (11%)	H-9->LUMO (7%), HOMO->L+10 (2%)
16	26107.3603123	383.033745288	0.0114	H-4->L+6 (49%)	H-10->LUMO (5%), H-4->L+1 (2%), H-4->L+7 (6%), H-4->L+10 (7%), H-3->L+1 (5%), H-1->L+1 (2%), H-1->L+2 (5%)
17	26251.7335551	380.927224445	0.0742	H-10->LUMO (11%), H-3->L+6 (35%)	H-16->L+6 (4%), H-10->L+6 (2%), H-9->LUMO (3%), H-4->L+6 (5%), H-3->L+1 (7%), H-3->L+7 (4%), H-3->L+10 (5%)
18	26582.420871	376.188461109	0.0068	H-1->L+2 (79%)	H-4->L+6 (4%), H-3->L+1 (3%), H-1->L+1 (5%)
19	27313.1591837	366.123886759	0.0048	H-12->LUMO (47%), H-11->LUMO (49%)	
20	27959.2092813	357.663905992	0.0181	H-3->L+1 (74%)	H-17->LUMO (3%), H-4->L+1 (2%), H-3->L+6 (4%), H-2->L+1 (3%)
21	28186.6576303	354.777786397	0.0003	H-12->LUMO (51%), H-11->LUMO (48%)	
22	28338.2898629	352.879445033	0.0018	H-17->LUMO (49%), H-4->L+1 (15%)	H-16->LUMO (9%), H-15->LUMO (6%), H-14->LUMO (8%), H-4->L+2 (5%), H-3->L+1 (4%)
23	28425.3977412	351.798067736	0.0036	H-17->LUMO (14%), H-4->L+1 (58%), H-4->L+2 (14%)	H-16->LUMO (4%), H-14->LUMO (2%)
24	29207.7555374	342.374818469	0.1099	H-2->L+1 (63%)	H-13->LUMO (8%), H-12-

					>L+1 (6%), H-11->L+1 (3%), H-3->L+1 (4%), H-2->L+2 (5%)
25	29667.4915619	337.06927932	0.1279	H-15->LUMO (67%)	H-17->LUMO (4%), H-16->LUMO (5%), H-13->LUMO (8%), H-3->L+2 (3%), H-2->L+1 (2%)
26	30047.378698	332.807733431	0.035	H-3->L+2 (10%), HOMO->L+6 (41%)	H-17->LUMO (2%), H-17->L+6 (7%), H-15->LUMO (6%), H-13->LUMO (3%), HOMO->L+5 (2%), HOMO->L+7 (4%), HOMO->L+10 (6%)
27	30274.0204925	330.316219561	0.035	H-14->LUMO (12%), H-13->LUMO (10%), H-12->L+1 (19%), H-11->L+1 (12%), HOMO->L+6 (10%)	H-17->LUMO (2%), H-15->LUMO (2%), H-3->L+2 (7%), H-2->L+2 (9%)
28	30452.2690213	328.382755091	0.1102	H-12->L+1 (21%), H-11->L+1 (14%), H-4->L+2 (11%), H-3->L+2 (20%)	H-14->LUMO (4%), H-13->LUMO (5%), H-4->L+1 (3%), H-2->L+1 (7%), HOMO->L+6 (2%)
29	30599.0619274	326.807404218	0.0063	H-4->L+1 (13%), H-4->L+2 (60%)	H-12->L+1 (3%), H-3->L+2 (8%), HOMO->L+6 (2%)
30	30679.7173703	325.948243894	0.0434	H-16->LUMO (60%), H-14->LUMO (13%)	H-17->LUMO (6%), H-13->LUMO (4%), H-4->L+2 (3%)
31	30697.4615677	325.759834504	0.0134	H-17->LUMO (14%), H-16->LUMO (11%), H-14->LUMO (45%), H-3->L+2 (15%)	H-15->LUMO (2%)
32	31437.0719791	318.095782159	0.0134	H-2->L+2 (76%)	H-14->LUMO (3%), H-13->LUMO (6%), H-2->L+1 (2%)
33	31631.4515965	316.14103986	0.0081	H-17->L+6 (42%), HOMO->L+6 (11%)	H-17->L+7 (5%), H-17->L+10 (7%), H-16->L+6 (7%), HOMO->L+3 (4%)
34	31715.3332571	315.304900596	0.0194	HOMO->L+3 (82%)	HOMO->L+6 (6%)
35	32451.7174508	308.150100689	0.6267	H-13->LUMO (11%), H-5->L+1 (25%), H-3->L+2 (11%), HOMO->L+4 (27%)	H-15->LUMO (2%), H-14->LUMO (4%), H-2->L+1 (4%), HOMO->L+2 (4%)
36	32603.3496835	306.716950776	0.201	H-5->L+1 (71%), HOMO->L+4 (13%)	H-3->L+2 (3%), H-2->L+1 (3%)
37	32784.82443	305.019171945	0.077	HOMO->L+4 (13%), HOMO->L+5 (72%)	HOMO->L+6 (8%)
38	32884.8371792	304.091516267	0.463	HOMO->L+4 (35%), HOMO->L+5 (21%)	H-14->LUMO (3%), H-13->LUMO (9%), H-3->L+2 (6%), H-2->L+1 (2%), HOMO->L+2 (4%), HOMO->L+7 (4%), HOMO->L+10 (3%)
39	33266.3374241	300.604177506	0.0241	H-7->L+1 (75%), H-6->L+1 (21%)	
40	34076.9246252	293.453711272	0.0025	H-7->L+1 (22%), H-6->L+1 (66%)	H-10->L+1 (6%), H-6->L+2 (3%)

41	34347.9269134	291.138385883	0.0102	H-10->L+1 (66%), H-8->L+1 (10%)	H-9->L+1 (7%), H-6->L+1 (7%), HOMO->L+7 (2%)
42	34548.7589662	289.445997461	0.0058	H-9->L+1 (84%)	H-10->L+1 (8%)
43	34799.5973936	287.359646345	0.0203	H-8->L+1 (73%), HOMO->L+7 (12%)	H-10->L+1 (3%), H-9->L+1 (5%), H-8->L+2 (2%)
44	34857.6693125	286.880913074	0.0956	H-8->L+1 (12%), HOMO->L+7 (47%), HOMO->L+9 (12%)	H-10->L+1 (8%), HOMO->L+4 (3%), HOMO->L+8 (8%)
45	34989.1376844	285.802985206	0.0336	HOMO->L+7 (13%), HOMO->L+8 (73%)	HOMO->L+9 (3%), HOMO->L+10 (4%)
46	35179.4845297	284.256581178	0.0526	H-1->L+3 (39%), H-1->L+4 (25%), HOMO->L+9 (10%)	H-1->L+10 (8%), HOMO->L+8 (4%)
47	35344.8281876	282.926824454	0.0371	HOMO->L+9 (67%)	H-1->L+3 (5%), H-1->L+4 (3%), HOMO->L+7 (7%), HOMO->L+8 (7%), HOMO->L+10 (4%)
48	35969.9078701	278.010164388	0.2437	H-5->L+2 (28%), HOMO->L+10 (47%)	H-9->L+2 (2%), HOMO->L+6 (4%), HOMO->L+8 (3%)
49	36260.2674646	275.783955807	0.1	H-5->L+2 (59%), HOMO->L+10 (18%)	H-12->L+1 (2%), H-11->L+1 (4%)
50	36471.584725	274.186056773	0.0081	H-12->L+1 (28%), H-11->L+1 (46%)	H-5->L+2 (5%), H-2->L+3 (5%), H-2->L+4 (8%)

Table S2. TD-DFT Calculated Electronic Transitions for **3a**.

HOMO is 196

No.	**Energy (cm-1)**	**Wavelength (nm)**	**Osc. Strength**	**Major contribs**	**Minor contribs**
1	6337.09814865	1578.00932942	0.0006	HOMO->LUMO (99%)	
2	9931.91123871	1006.85555475	0.0018	H-1->LUMO (98%)	
3	11452.2663374	873.189612031	0.0008	H-2->LUMO (98%)	
4	13060.5358688	765.665367827	0.0021	H-3->LUMO (99%)	
5	19482.3222325	513.285833211	0.1217	H-4->LUMO (86%)	HOMO->L+1 (9%)
6	19838.8192901	504.062255609	0.0001	H-6->LUMO (81%), H-5->LUMO (16%)	
7	20175.9590414	495.639388416	0.0055	H-7->LUMO (25%), H-5->LUMO (33%), HOMO->L+1 (29%)	H-6->LUMO (8%)
8	20747.8061316	481.978669772	0.0051	H-7->LUMO (42%), H-5->LUMO (41%)	H-8->LUMO (2%), H-6->LUMO (9%), HOMO->L+1 (3%)
9	20935.7333136	477.652244143	0.0015	H-8->LUMO (90%)	H-9->LUMO (4%), H-7->LUMO (4%)
10	21034.1329539	475.417742292	0.0268	H-9->LUMO (77%)	H-7->LUMO (7%), H-5->LUMO (2%), HOMO->L+1 (7%)
11	22440.7638781	445.617629343	0.0589	HOMO->L+2 (71%)	H-10->LUMO (2%), H-9-

					>LUMO (6%), H-7->LUMO (3%), H-1->L+1 (7%), HOMO->L+1 (6%)
12	22674.6646625	441.020855164	0.0032	H-1->L+1 (84%), HOMO->L+2 (10%)	H-2->L+1 (3%)
13	23331.1999677	428.610616421	0.1824	H-10->LUMO (41%), HOMO->L+1 (12%), HOMO->L+2 (14%)	H-9->LUMO (5%), H-7->LUMO (8%), H-5->LUMO (2%), H-4->LUMO (5%), H-1->L+1 (2%)
14	24220.8295029	412.867775598	0.0005	H-1->L+7 (12%), H-1->L+8 (45%), H-1->L+9 (17%)	H-15->L+8 (5%), H-2->L+1 (6%)
15	24309.5504901	411.360958899	0.0007	H-2->L+1 (80%)	H-3->L+8 (3%), H-1->L+1 (4%), H-1->L+8 (3%)
16	25526.6411234	391.74758448	0.0245	H-12->LUMO (13%), H-11->LUMO (61%)	H-16->LUMO (7%), H-13->LUMO (4%), H-3->L+1 (6%)
17	25599.231022	390.636734025	0.0032	H-3->L+1 (79%)	H-11->LUMO (6%), H-2->L+8 (5%)
18	26085.5833427	383.353512498	0.0023	H-16->LUMO (47%), H-13->LUMO (17%), H-11->LUMO (12%)	H-14->LUMO (6%), H-3->L+1 (3%), H-2->L+8 (5%)
19	26370.2970562	379.214537428	0.0123	H-13->LUMO (13%), H-2->L+8 (31%), H-2->L+9 (12%)	H-17->L+8 (4%), H-14->LUMO (7%), H-12->LUMO (4%), H-3->L+1 (8%), H-2->L+7 (7%)
20	26438.0476282	378.24275607	0.008	H-16->LUMO (36%), H-13->LUMO (20%), H-12->LUMO (17%)	H-15->LUMO (3%), H-14->LUMO (3%), H-2->L+8 (4%), H-1->L+2 (5%)
21	26619.5223747	375.664140747	0.0007	H-3->L+8 (14%), H-1->L+2 (62%)	H-12->LUMO (3%), H-3->L+7 (4%), H-3->L+9 (5%)
22	26849.390387	372.44793479	0.0366	H-13->LUMO (17%), H-12->LUMO (54%), H-11->LUMO (12%)	H-16->LUMO (2%), H-14->LUMO (9%)
23	27088.130498	369.165380415	0.5338	H-15->LUMO (12%), H-14->LUMO (14%), H-10->LUMO (30%)	H-13->LUMO (8%), H-12->LUMO (6%), H-7->LUMO (2%), HOMO->L+1 (8%)
24	27414.7850417	364.766675529	0.0339	H-3->L+7 (10%), H-3->L+8 (35%), H-3->L+9 (13%), H-1->L+2 (27%)	H-2->L+1 (3%), H-2->L+2 (2%)
25	27865.6489675	358.864780492	0.3171	H-15->LUMO (48%), H-14->LUMO (12%)	H-18->LUMO (2%), H-16->LUMO (3%), H-10->LUMO (8%), H-7->LUMO (2%), H-2->L+2 (2%), HOMO->L+1 (8%)
26	29161.7819349	342.914572995	0.0663	H-17->LUMO (73%)	H-15->LUMO (9%), H-14->LUMO (9%), H-13->LUMO (2%)
27	29337.6108004	340.859385859	0.167	H-2->L+2 (82%)	H-15->LUMO (4%), H-14-

					>LUMO (2%), H-13->LUMO (3%)
28	30352.2562721	329.464798608	0.4404	H-17->LUMO (19%), H-15->LUMO (18%), H-14->LUMO (24%)	H-18->LUMO (6%), H-13->LUMO (5%), H-2->L+2 (7%), HOMO->L+1 (4%)
29	30811.9922967	324.548958202	0.015	H-3->L+2 (96%)	
30	31563.7010245	316.819627465	0.0182	H-4->L+1 (58%), HOMO->L+3 (25%)	H-5->L+1 (4%), HOMO->L+4 (3%)
31	31705.654604	315.40115241	0.0174	H-16->L+8 (10%), H-4->L+1 (19%), HOMO->L+3 (36%), HOMO->L+8 (11%)	H-16->L+7 (3%), H-16->L+9 (4%), HOMO->L+6 (2%), HOMO->L+7 (5%), HOMO->L+9 (3%)
32	31837.9295303	314.090776238	0.0034	H-16->L+8 (23%), HOMO->L+3 (32%), HOMO->L+8 (12%)	H-16->L+7 (6%), H-16->L+9 (8%), H-4->L+1 (4%), HOMO->L+9 (6%)
33	32204.1052411	310.519417482	0.0025	H-6->L+1 (70%), H-5->L+1 (17%)	H-11->L+2 (5%)
34	32278.3082486	309.805579741	0.0044	H-16->L+8 (15%), HOMO->L+4 (38%), HOMO->L+8 (15%)	H-16->L+7 (4%), H-16->L+9 (6%), HOMO->L+3 (2%), HOMO->L+7 (4%), HOMO->L+9 (7%)
35	32295.2458916	309.643098355	0.0069	H-11->L+1 (10%), H-11->L+2 (46%), H-6->L+1 (11%)	H-12->L+2 (9%), H-11->LUMO (2%), H-10->L+2 (4%), H-4->L+2 (4%)
36	32451.7174508	308.150100689	0.0034	HOMO->L+4 (53%), HOMO->L+8 (19%)	H-16->L+8 (6%), H-16->L+9 (2%), HOMO->L+7 (5%), HOMO->L+9 (5%)
37	32554.1498633	307.180499014	0.0236	H-18->LUMO (15%), H-9->L+1 (10%), H-6->L+1 (10%), H-5->L+1 (46%)	H-7->L+1 (6%), H-4->L+1 (4%)
38	32771.1130047	305.146791889	0.0169	H-18->LUMO (10%), H-9->L+1 (12%), H-7->L+1 (38%), H-5->L+1 (24%)	H-8->L+1 (5%), H-6->L+1 (5%)
39	33129.2231712	301.84830922	0.0	H-8->L+1 (80%), H-7->L+1 (17%)	
40	33259.8849887	300.662494877	0.0841	H-18->LUMO (26%), H-9->L+1 (18%), HOMO->L+5 (33%), HOMO->L+6 (12%)	
41	33333.2814417	300.000467025	0.0438	H-18->LUMO (12%), H-9->L+1 (12%), HOMO->L+5 (61%)	HOMO->L+6 (6%), HOMO->L+8 (2%)
42	33508.3037528	298.433489017	0.004	H-9->L+1 (41%), H-7->L+1 (21%), HOMO->L+6 (17%)	H-8->L+1 (9%), H-4->L+1 (4%)
43	34222.1044225	292.208798049	0.225	H-4->L+2 (80%)	H-7->L+1 (3%), HOMO->L+6 (5%)
44	34398.7398424	290.708323788	0.1037	H-19->LUMO (27%), HOMO->L+6 (35%)	H-18->LUMO (9%), H-7->L+1 (2%), H-4->L+2 (9%)
45	34490.6870473	289.933337259	0.099	H-19->LUMO (63%), HOMO->L+6 (16%)	H-21->LUMO (2%), H-18->LUMO (6%)

46	35337.5691978	282.984942853	0.0587	H-5->L+2 (76%)	H-7->L+2 (2%), H-6->L+2 (8%), HOMO->L+7 (6%)
47	35406.9328787	282.430563366	0.1282	HOMO->L+7 (69%), HOMO->L+8 (17%)	H-5->L+2 (7%)
48	35635.1877821	280.62150426	0.0728	HOMO->L+8 (19%), HOMO->L+9 (69%)	H-10->L+1 (5%), H-7->L+2 (2%)
49	35875.5410019	278.741441125	0.0127	H-10->L+1 (14%), H-7->L+2 (56%)	H-8->L+2 (6%), H-5->L+2 (3%), HOMO->L+9 (4%), HOMO->L+10 (5%)
50	36086.8582623	277.109188262	0.0484	H-10->L+1 (24%), H-7->L+2 (14%), HOMO->L+10 (44%)	H-1->L+3 (3%), H-1->L+6 (2%)

Table S3. NICS(*z*) (in ppm) for DFT-optimized structures of **2a**, **3a**, **1b**, **1c**, and substituted pyrazole **pz** and pyrazoline **pz**-H2, calculated at the geometric center and in the distance of *z* Å from the mean plane of each ring specified with red letter.

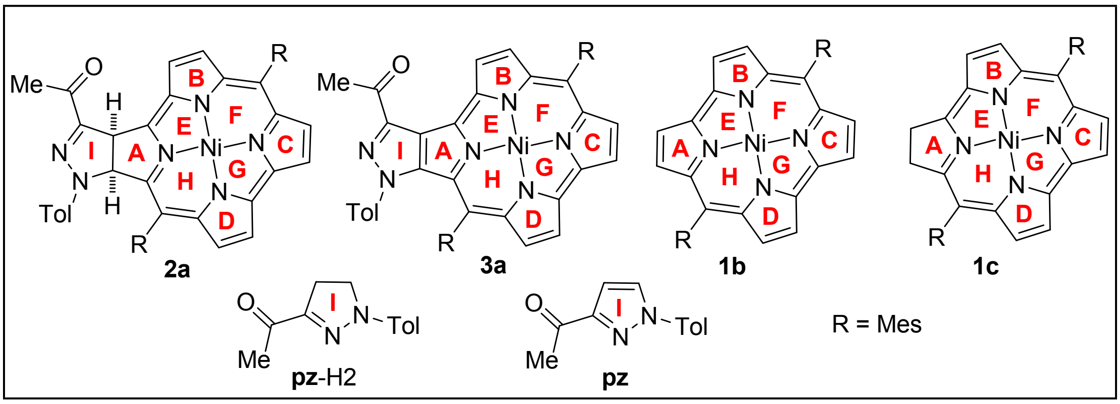

ring	*z*[a]	**2a**	**3a**	**1c**	**1b**	**pz**	**pz**-H2
A	-1	-6.65	4.85	-8.47	7.73		
A	0	-10.37	2.52	-12.05	6.07		
A	1	-10.91	-0.03	-12.36	2.37		
B	-1	4.84	8.94	3.84	7.73		
B	0	1.52	6.70	1.16	6.07		
B	1	-1.94	3.10	-1.32	2.37		
C	-1	8.94	10.87	8.65	7.74		
C	0	9.41	9.44	9.44	6.08		
C	1	4.44	4.81	4.45	2.38		
D	-1	9.83	11.85	10.22	7.74		
D	0	7.18	8.42	8.81	6.08		
D	1	2.52	3.54	4.69	2.38		
E	-1	34.77	47.16	34.33	40.25		
E	0	35.35	50.36	36.78	43.38		
E	1	25.18	39.62	27.67	33.86		
F	-1	30.38	44.44	29.76	38.06		
F	0	34.20	50.42	33.86	43.17		
F	1	25.41	39.03	25.55	33.34		
G	-1	30.93	45.81	31.55	40.25		
G	0	31.23	48.53	32.50	43.37		
G	1	23.86	37.74	25.80	33.86		
H	-1	27.37	42.17	28.30	38.06		
H	0	29.59	46.86	31.65	43.17		
H	1	21.87	36.57	24.03	33.34		
I	-1	-5.39	-6.33			-10.73	-2.34
I	0	-5.98	-7.34			-11.91	-1.92
I	1	-6.46	-7.86			-10.88	-2.34

[a] Convex side of norcorrole ring facing upwards corresponds to positive *z*.

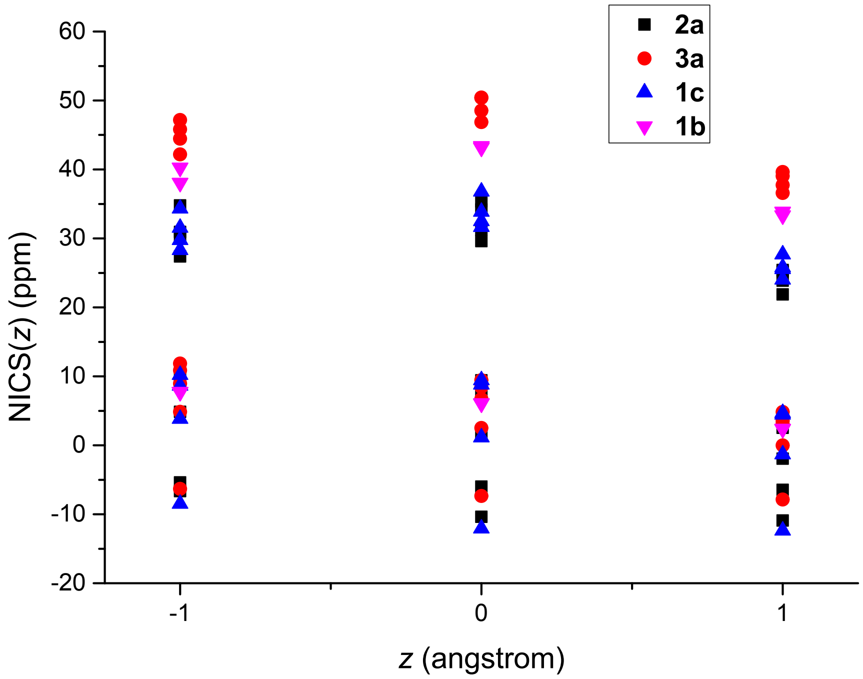

Figure S32. NICS values calculated at different distances from the mean planes of conjugated rings of the systems specified.

Table S4. Computational details for structures discussed in the paper. Optimizations were performed at the PCM(CH_2Cl_2)/B3LYP/6-31G(d,p) level of theory.

Structure	**Code**[a]	**SCF *E***[b]	**ZPV**[c]	**lowest freq.** [d]	***G***[e]	**HOMO**	**LUMO**	**HLG**
		a.u.	a.u.	cm^{-1}	a.u.	eV	eV	eV
1b	cof_norco	-3117.2136124	0.564541	13.66	-3116.720007	-4.89	-3.37	1.51
1c	cof_norco_chlorin	-3118.4317454	0.588194	14.28	-3117.914587	-4.60	-3.01	1.59
2a	cof_2a_MM	-3689.0276157	0.750357	11.99	-3688.364582	-4.74	-3.12	1.62
3a	cof_3a_MM	-3687.8332153	0.726894	10.85	-3687.193437	-4.83	-3.38	1.45

[a] Optimized geometry available as <code>.pdb file. [b] Electronic energy. [c] Zero-point vibrational energy. [d] Lowest vibrational frequency. [e] Gibbs free energy.

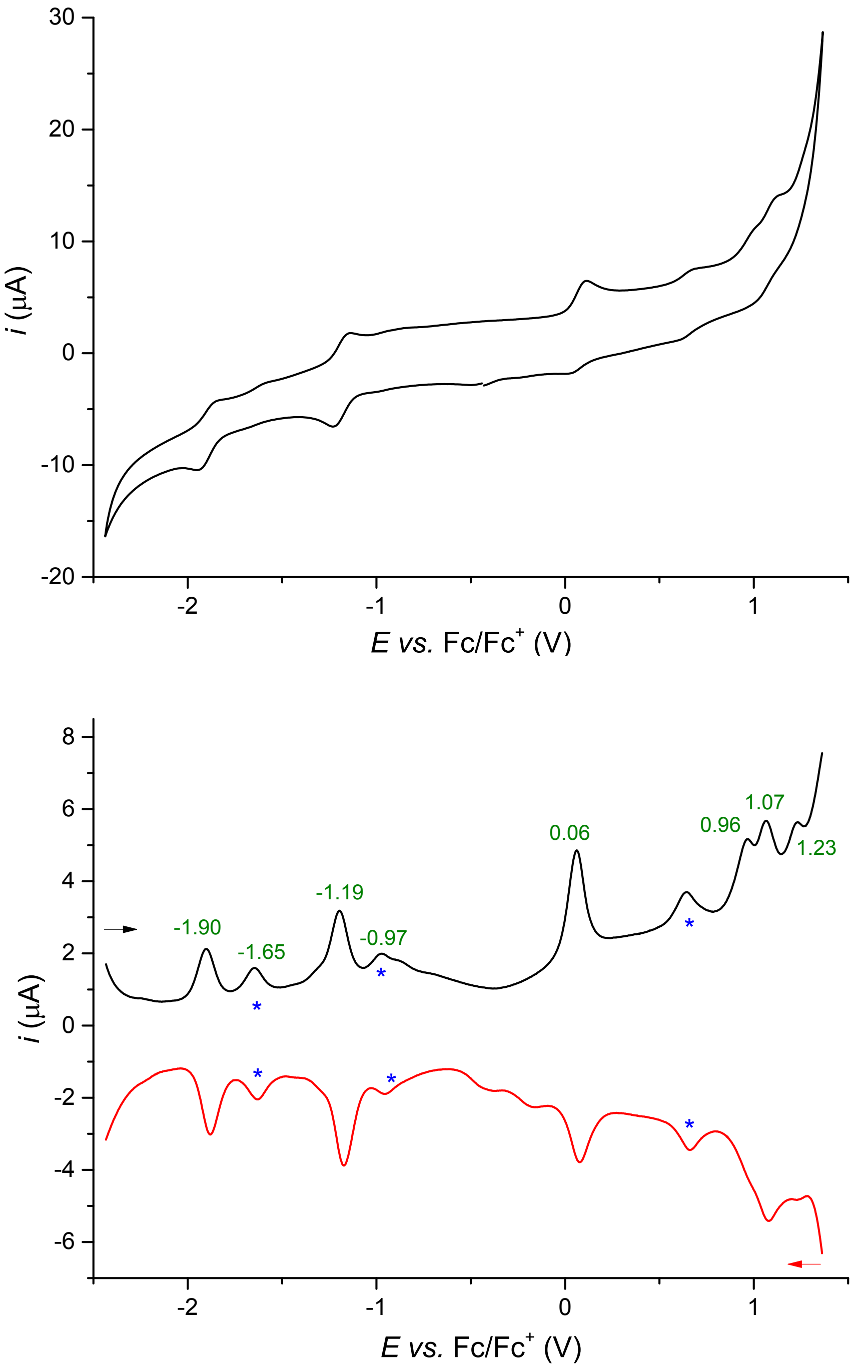

Figure S33. Cyclic (top) and differential pulse (bottom) voltammograms of **2a** (DCM, $[BuN_4]PF_6$). Features marked with blue asterisks are due to dehydrogenation product **3a** which is formed *in situ* upon the measurement.

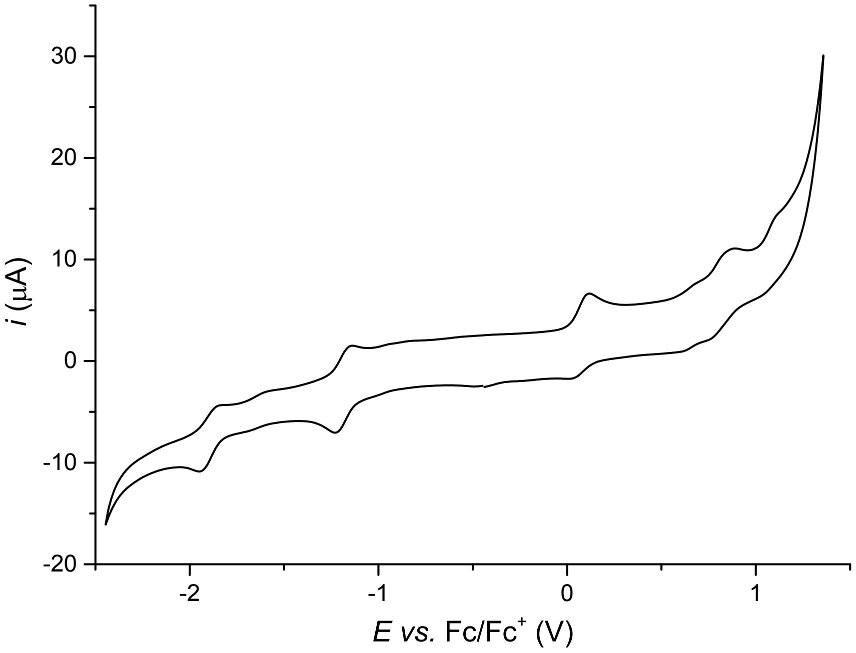

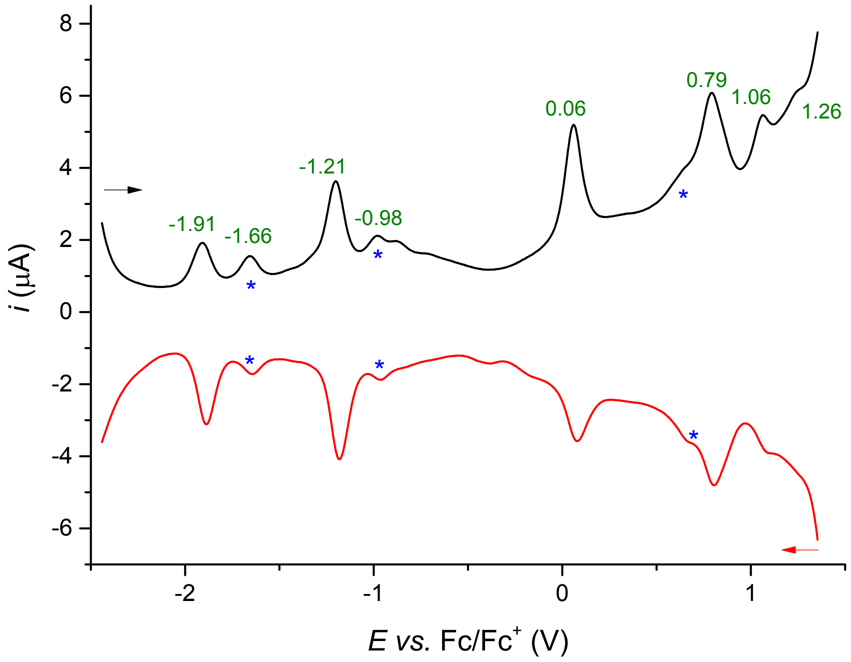

Figure S34. Cyclic (top) and differential pulse (bottom) voltammograms of **2b** (DCM, [BuN$_4$]PF$_6$). Features marked with blue asterisks are due to dehydrogenation product **3b** which is formed *in situ* upon the measurement.

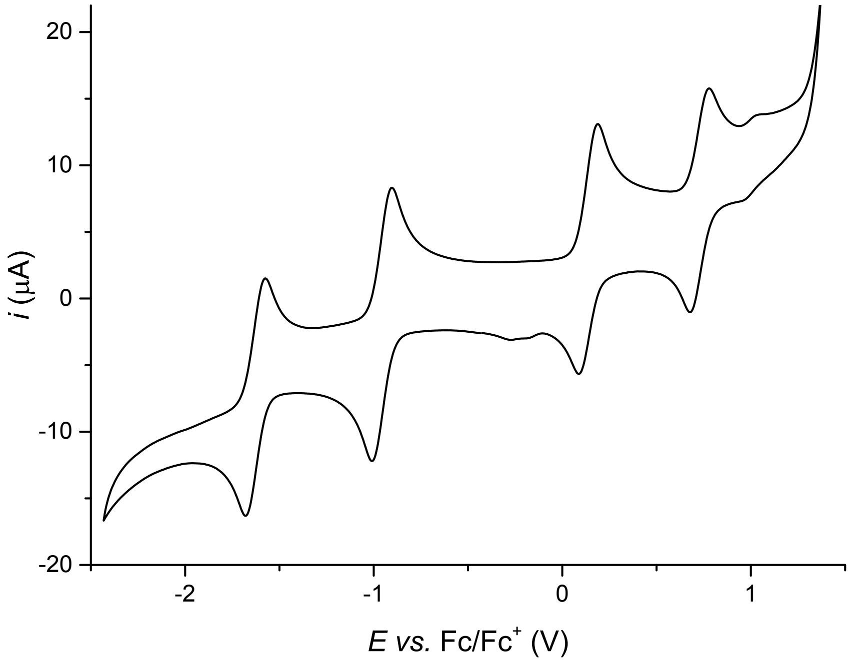

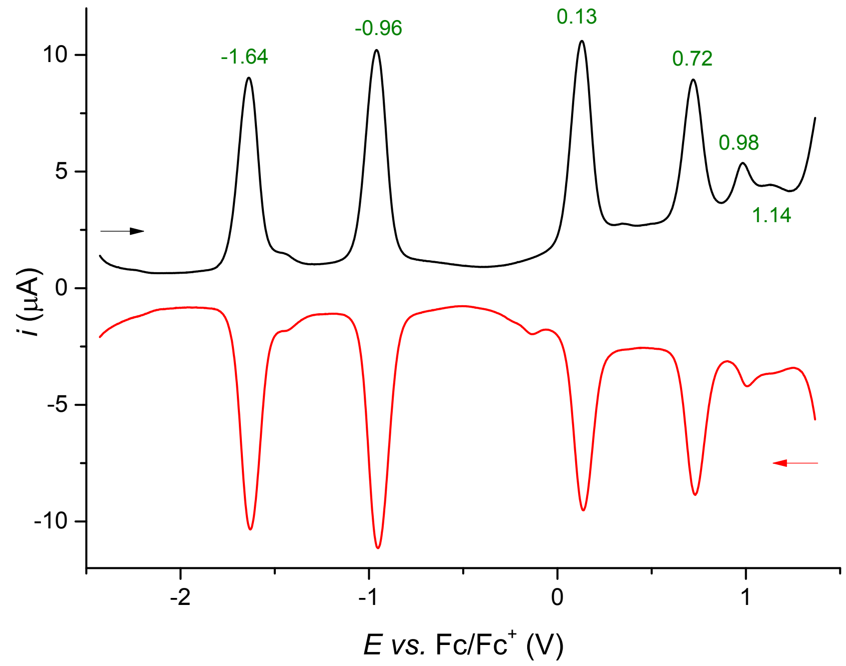

Figure S35. Cyclic (top) and differential pulse (bottom) voltammograms of **3a** (DCM, $[BuN_4]PF_6$).

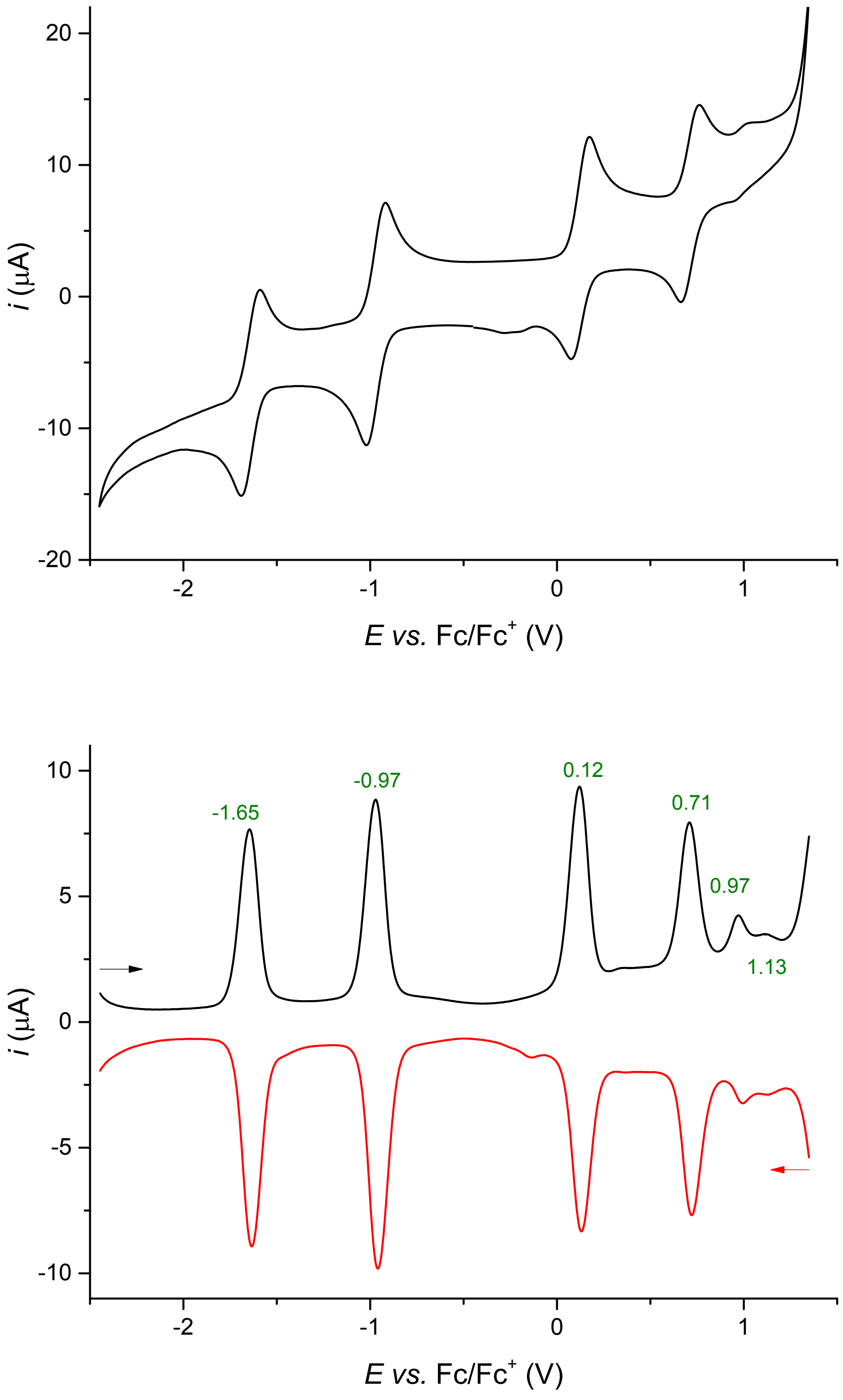

Figure S36. Cyclic (top) and differential pulse (bottom) voltammograms of **3b** (DCM, $[BuN_4]PF_6$).

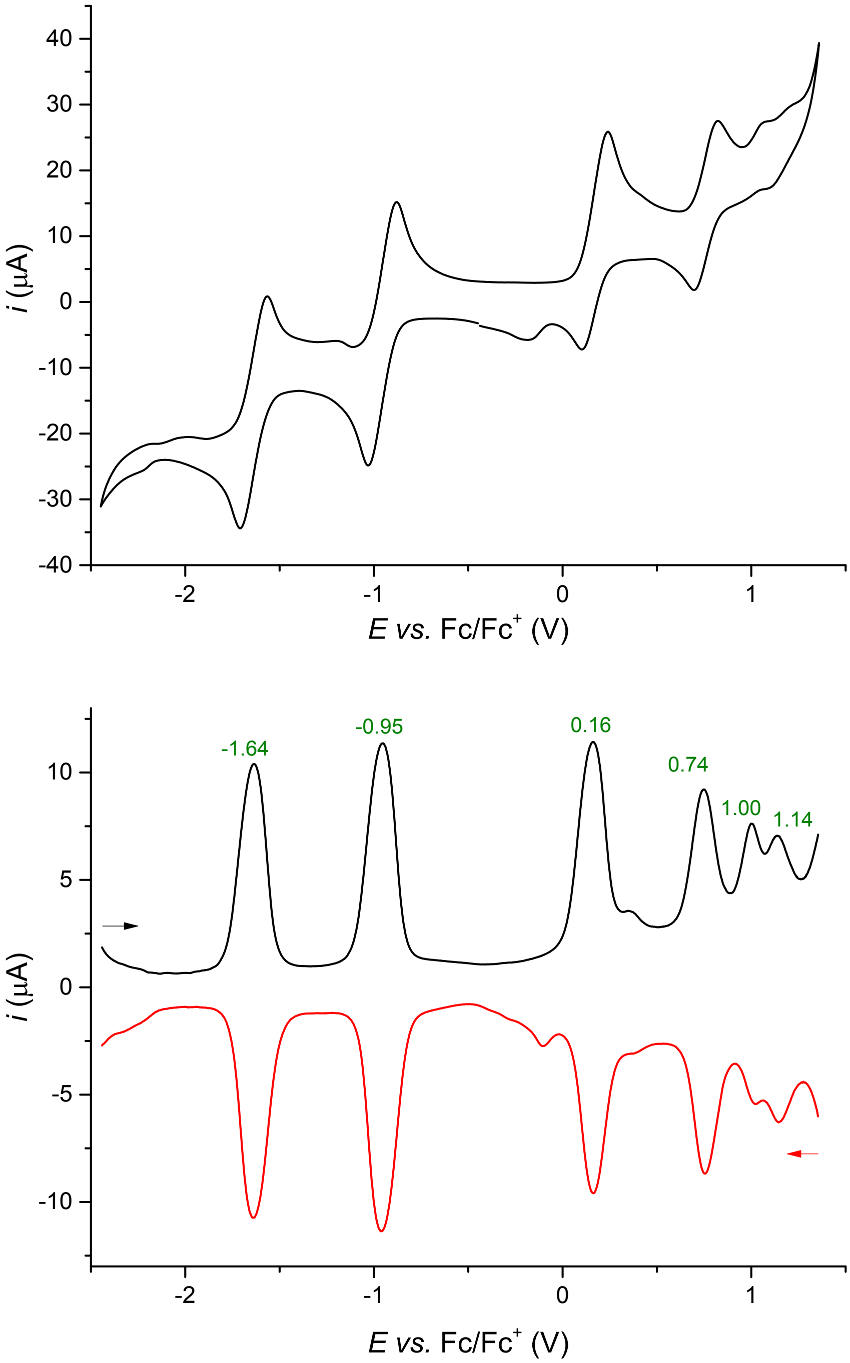

Figure S37. Cyclic (top) and differential pulse (bottom) voltammograms of **3c** (DCM, $[BuN_4]PF_6$).

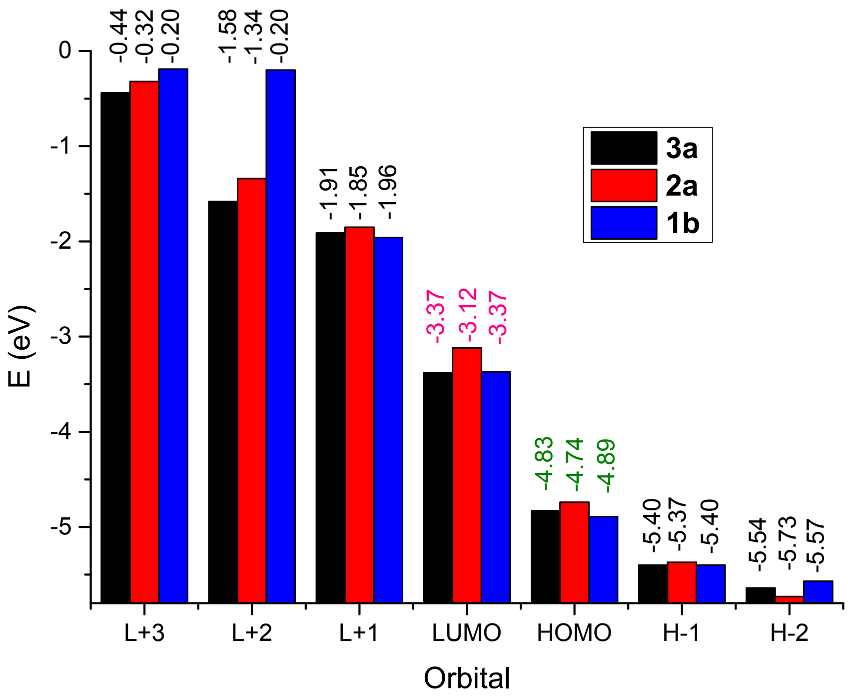

Figure S38. Energies of Kohn-Sham frontier orbitals calculated for **2a**, **3a**, and **1b**.

Reference List

1. G. M. Sheldrick, *Acta Cryst.*, 2008**, A64**, 112.
2. C. B. Hübschle, G. M. Sheldrick, and B. Dittrich, *J.Appl.Cryst.*, 2011**, 44**, 1281.
3. Frisch, M. J.; Trucks, G. W.; Schlegel, H. B.; Scuseria, G. E.; Robb, M. A.; Cheeseman, J. R.; Scalmani, G.; Barone, V.; Mennucci, B.; Petersson, G. A.; Nakatsuji, H.; Caricato, M.; Li, X.; Hratchian, H. P.; Izmaylov, A. F.; Bloino, J.; Zheng, G.; Sonnenberg, J. L.; Hada, M.; Ehara, M.; Toyota, K.; Fukuda, R.; Hasegawa, J.; Ishida, M.; Nakajima, T.; Honda, Y.; Kitao, O.; Nakai, H.; Vreven, T.; Montgomery, Jr., J. A.; Peralta, J. E.; Ogliaro, F.; Bearpark, M.; Heyd, J. J.; Brothers, E.; Kudin, K. N.; Staroverov, V. N.; Kobayashi, R.; Normand, J.; Raghavachari, K.; Rendell, A.; Burant, J. C.; Iyengar, S. S.; Tomasi, J.; Cossi, M.; Rega, N.; Millam, J. M.; Klene, M.; Knox, J. E.; Cross, J. B.; Bakken, V.; Adamo, C.; Jaramillo, J.; Gomperts, R.; Stratmann, R. E.; Yazyev, O.; Austin, A. J.; Cammi, R.; Pomelli, C.; Ochterski, J. W.; Martin, R. L.; Morokuma, K.; Zakrzewski, V. G.; Voth, G. A.; Salvador, P.; Dannenberg, J. J.; Dapprich, S.; Daniels, A. D.; Farkas, Ö.; Foresman, J. B.; Ortiz, J. V.; Cioslowski, J.; Fox, D. J. Gaussian 09 Revision B.01.
4. A. D. Becke, *Phys.Rev.A*, 1988**, 38**, 3098.
5. A. D. Becke, *J.Chem.Phys.*, 1993**, 98**, 5648.
6. C. Lee, W. Yang, and R. G. Parr, *Phys.Rev.B*, 1988**, 37**, 785.
7. J.-D. Chai and M. Head-Gordon, *Phys.Chem.Chem.Phys*, 2008**, 10**, 6615.
8. L. E. Roy, P. J. Hay, and R. L. Martin, *J.Chem.Theory Comput.*, 2008**, 4**, 1029.
9. N. M. O'Boyle, A. L. Tenderholt, and K. M. Langner, *J.Comp.Chem.*, 2008**, 29**, 839.
10. T. Ito, Y. Hayashi, S. Shimizu, J.-Y. Shin, N. Kobayashi, and H. Shinokubo, *Angew.Chem.Int.Ed.*, 2012**, 51**, 8542.